NEUTRONICS SIMULATIONS OF GRAPHITE EXPERIMENTS

A Thesis

by

LANCE WILLIAM MERCHANT

Submitted to the Office of Graduate and Professional Studies of
Texas A&M University
in partial fulfillment of the requirements for the degree of

MASTER OF SCIENCE

Chair of Committee,	Marvin Adams
Co-Chair of Committee,	Ryan McClarren
Committee Member,	Lawrence Rauchwerger
Head of Department,	Yassin Hassan

December 2016

Major Subject: Nuclear Engineering

Copyright 2016 Lance William Merchant

ABSTRACT

A widely used method for Neutronics simulations is MCNP6. Throughout this work, multiple MCNP6 simulations were completed on different supercomputers. These simulations entailed realistic representations of experiments being completed. The IM1 configuration was simulated with the corrected source definition. This geometry resulted in 0.222 as the graphite to air ratio. The IM1 experiment required many different configurations to be modeled in MCNP6. In order to further characterize the experiment different boric acid concentrations were poured in a beaker. The boric acid concentration produced an exponential fit, this represented the decrease in absorptions per second as the boric acid concentration was increased. With the progression of the project a more complex problem was created. This year 5 geometry was approached primarily through a straightforward stacked air duct problem. These results concluded that with the addition of a more complex geometry MCNP6 would require many neutron particle histories and become computationally expensive. Finally, in anticipation of the arrival of the neutron generator safety calculations were completed. These calculations yielded an estimated dose of 107.04 ± 0.3 mrem per hour in the entrance way during operation. The estimated dose was less than 5 mrem per hour in every other location of concern. The geometries were developed in MCNP6 and converted into PDT readable formats. This work was completed in order to aid in the validation of PDT development.

ACKNOWLEDGEMENTS

I would like to respectfully thank my co-committee chairs, Dr. Marvin Adams and Dr. Ryan McClarren, and my committee member, Dr. Lawrence Rauchwerger, for their leadership and mentorship throughout the entirety of this work and my graduate career. This research could not have been completed without the sponsorship of the Center for Exascale Radiation Transport; I greatly appreciate their funding and vision for future applications.

I would like to recognize the faculty and staff at Texas A&M University Nuclear Engineering for the dedication and support to foster a learning environment in which all the research and course work was made possible. Specifically, I would like to express gratitude to my peers, Simon Bolding, Jacob Landman, and Richard Vega for their help with certain aspects of this project and my sanity.

Finally, I would like to recognize my mother, father and sister for the moral support and motivation to complete what has been a lifelong goal. I would also like to thank Katherine Holland for her support, care, and love throughout the long nights and tireless effort completing this nuclear engineering masters project.

NOMENCLATURE

AmBe	Americium- Beryllium
LANL	Los Alamos National Laboratory
LLNL	Lawrence Livermore National Laboratory
MCNP6	Monte Carlo N-Particle Code
PDT	Parallel Deterministic Transport
TAMU	Texas A&M University

TABLE OF CONTENTS

Page

LIST OF FIGURES

Page

LIST OF TABLES

Page

1. INTRODUCTION

The development of a new code requires many hours of tireless work and dedication. In the stages of development, it is important for the code to have experimental and simulation validation. At Texas A&M University a 3-D particle transport code, PDT, is being developed. This deterministic solver utilizes the discrete ordinates approximation (S_n), the multigroup approximation in energy, and will allow for general polyhedral spatial meshing. To aid the development of PDT experiments were completed. In support of these experiments Monte Carlo simulations were completed in order to serve as another form of validation for the PDT solver. Monte Carlo N-Particle code (MCNP6) is widely used to simulate how neutrons and other particles interact with different materials given specific boundary and initial conditions. MCNP6 is a general-purpose, continuous-energy, generalized-geometry, time-dependent, Monte Carlo radiation-transport code designed to track many particle types over a broad range of energies (Los Alamos National Laboratory). MCNP6 has been tested and an efficient means to develop geometries that can represent experimental configurations with high accuracy. MCNP6 calculations require many particles histories sampled in order to produce the high fidelity results needed. Throughout this project supercomputing facilities at both Los Alamos National Laboratory (LANL) and Lawrence Livermore National Laboratory (LLNL) were used. Most simulations were completed in under two hours utilizing 320 processers on CAB, a supercomputer located at LLNL. The results obtained from MCNP6 calculations are always associated with a given uncertainty. It is this uncertainty value that was needed to be decreased to validate the PDT results. In order to decrease the uncertainty associated

with the MCNP6 results a large amount of computational time was needed. MCNP6 results aided in the validation of experimental results coupled with PDT simulations. The following work focuses on three main topics to be expanded upon: Impurities Model 1 (IM1), Year 5 Experimental Configuration, and Neutron Generator Safety Calculations.

1.1 Simulations Strategy

The first group of simulations that were completed explored the impurities within the different graphite blocks. An MCNP6 input deck was utilized to represent the most up to date experimental setup of IM1. This setup consists of an Americium Beryllium (AmBe) neutron source located at the bottom of a polyethylene cylinder, which rests on top of a wood table. A block of graphite or a beaker filled with boric acid is place above the cylinder. In addition, the Boron Trifluoride (BF_3) neutron detector is located above the graphite or beaker.

The MCNP6 simulation was completed using the exact measurements acquired from the experimental setup. These dimensions were crucial in order to increase the confidence in the results. The first simulation consisted of the graphite block located in the standard position with the BF_3 detector positioned above it. In order to properly model the experiment, the AmBe source needed to be modeled as accurately as possible, given the information available. The graphite block on top of the polyethylene cylinder was transitioned into multiple configurations. In addition, the BF_3 detector was placed into various experimental setups. These different configurations allowed for additional insight in how experimental results aligned with MCNP6 and PDT simulations.

In an effort to further characterize the system, a beaker filled with different concentrations of boric acid was used in place of the graphite block. This allowed for higher confidence in the ability to predict the unknown impurities present in the graphite. The concentration of boric acid in the experiment and simulations was known.

During the IM1 experiment, neutrons scattering off the surrounding concrete needed to be taken into consideration. In order to decrease computational time when using PDT and MCNP6, the experiment was enclosed in a borated polyethylene box. This allowed for higher energy neutrons to escape the experiment; however, this would not allow them to scatter back into the detector region. This setup eliminated an experimental variable, and provided a higher confidence in the simulated results.

During the different experimental setups, an MCNP6 geometry was created to represent the experiment as realistically as possible. This geometry was converted into a format PDT could accept in order to produce a spatial mesh. Once this mesh was formed, the PDT simulation was completed and the results were compared. As part of this work, the MCNP6 simulations are reported as a means of validating the PDT results. The results obtained for the MCNP6 simulations reflected the neutron absorptions per second expected inside the BF_3 detector for each scenario.

The second group of simulations encompassed the different year 5 configurations. The year 5 experiment was a more challenging neutron experiment to model in MCNP6. The goal of the year 5 experiment was to use a neutron generator to pulse high energy neutrons into a graphite maze. The graphite maze was made up of air ducts as well as asymmetric air slits. These neutron streaming paths are outlets on the top and side of the

graphite stack. The neutron generator was on order during the completion of this project and therefore the AmBe neutron source that was used for the IM1 simulations was also used for the year 5 simulations.

The first approach of the year 5 experiment was to model a simple stacked air duct in a graphite stack. An AmBe neutron source was used in order to simulate the neutron streaming paths through these air ducts. This straightforward setup allowed for a rapid visualization of the neutron streaming paths. Due to the large neutron scattering cross-section in graphite, this simulation required an extensive amount of computational time. In an effort to reduce the relative standard error in the graphite maze, many neutron histories were sampled. The preliminary year 5 results consisted of multiple mesh grids that represented the track length estimate of the neutron flux averaged over each individual mesh cell in units of neutrons per cm^2 per source neutron. The estimate of the neutron flux averaged over each individual mesh grid was used in order to visualize the effect neutron streaming paths had on the geometry.

A more detailed year 5 experiment with the addition of air slits that spanned the height of the graphite maze was created. In order to better discriminate where neutrons were escaping the graphite maze, sixty detectors were modeled around the graphite stack. The simulated results complemented the upcoming experimental setup. Detectors should be placed in locations with the largest neutron escape probabilities in order to increase the experimental count rate. The results obtained from the more detailed year 5 MCNP6 simulations reflected the estimated neutron absorptions per second expected inside the BF_3 detector at each of the sixty locations.

The year 5 geometry created in MCNP6 was made available to be readily imported and meshed into a PDT format. This aided in the progression and validation of PDT, as this problem is more challenging than the previous. The IM1 experiment was able to rely on a one quarter geometry due to symmetry, however the year 5 experiment will have additional variables by the inclusion of a large graphite stack and asymmetric air slits.

The final group of simulations involved the neutron generator safety calculations. The neutron generator is cable of producing a pulse of 14.1 MeV neutrons 98% of the time and 2.5 MeV neutrons 2% of the time. The dose to operating and witnessing personnel was calculated. The neutron generator source was defined as accurately as possible given the available information. An MCNP6 geometry of the laboratory room was modeled. The MCNP6 simulation contained specific dose response functions. The dose in the adjoining room and the laboratory room entrance was simulated (Turner, 2007).

As simulations were finished the calculated dose was analyzed. Different shielding configurations were modeled in order to limit exposure of personnel to radiation. The purpose of this research is to provide the estimated doses an operator would receive at different locations throughout the lab space. The results obtained from the neutron generator safety simulations provided a dose in mrem per hour specific to certain areas in the laboratory space utilizing a phantom sphere in those locations.

1.2 Motivations

One of the main purposes of this work is to provide an up-to-date geometry for each experimental configuration completed or in progress. This geometry, created in MCNP6, allows for more efficient run times in PDT. Creating a meshed geometry from

scratch in PDT can be a very cumbersome experience. Through development at Texas A&M University a geometry can be created in MCNP6 and then converted and meshed into a PDT format rapidly. By using the same geometry user error is reduced as opposed to creating two separate geometries. This allows for higher confidence that the results being compared are from the same experimental setup.

The next main purpose of these simulations was to provide results to the PDT development team. The IM1 and year 5 simulations results provide an additional means to aid in the validation of PDT. By providing the simulated absorptions per second in the BF_3 detector values to the PDT development team the results can be compared. This information in conjunction with experimental results allows for further confidence in the PDT solver. This thesis covers the MCNP6 simulation results and does not address the comparison with PDT or experimental data.

The final motivation for this work derives from the neutron generator safety calculation. As a means to assist the experimentalist prepare for the arrival of the neutron generator an estimate of the dose was requested. The neutron generator is a device that has not been used before by the experimentalist and therefore a simulation of the estimated dose witnessing and operating personal would receive was calculated. These results provided a rough approximation of the dose and will be used to compliment additional safety measurements at which time the neutron generator arrives on site.

1.3 Thesis Organization

This thesis is divided up into four sections to detail the topic being supported and present the results obtained. Section 1 contains an introduction that provides an overview

of the simulations that were completed and the motivation behind the work. Section 2 thoroughly describes the experimental configuration for each of the three main simulations. This includes the IM1, year 5, and neutron generator safety configurations. Section 3 encompasses the results for each simulation. This is the prominent feature of the thesis and provides the reader with results from each simulation completed. This includes analysis on each source definition considered for the MCNP6 simulations, the different graphite experiments, boric acid experiments, year 5 configurations, and safety calculations with the addition of shielding. Section 6 contains the conclusion and future work in regards to the simulations completed. An appendix is attached that provides the does conversion table that was utilized.

2. EXPERIMENTAL DESCRIPTION

The purpose of this section is to describe the different geometries simulated using MCNP6. For each simulation the foundation of the geometry remained constant and minor variations allowed for additional insight in reaching the goal. The IM1 experiment utilized the same base structure for each simulation and involved a standard block of graphite. The year 5 simulation was modeled after a basic concept which had many changes due to the infancy of the project. The geometry for the safety calculations did not change as the exterior of the room was permanent, however the placement of shielding in or around the room was optimized. This section will go into detail on the experimental setup for each the IM1, year 5, and safety calculation geometries.

2.1 IM1 Geometry

The IM1 simulation of the geometry only changed slightly due to different experimental needs. The foundation of this geometry remained constant as the experimental configuration was already assembled. As the simulations were completed the experimental results were also completed, thus allowing for minor changes. The IM1 experiment utilized an AmBe neutron source during experimental trials. The AmBe source was defined as having an emission rate of 6.47×10^{6} neutrons per second. A typical AmBe source spectrum can be found in Figure 2.1 below. This spectrum is derived from ISO 8529-2. The AmBe source is distributed uniformly across the volume simulated in MCNP6 while staying true to the energies as described in Figure 2.1 as close as possible.

The standard IM1 geometry is represented in Figure 2.2. The XZ cross section of this geometry is represented in Figure 2.3 below. The YZ cross section of this geometry is represented in Figure 2.4 below. The different materials are represented by distinct

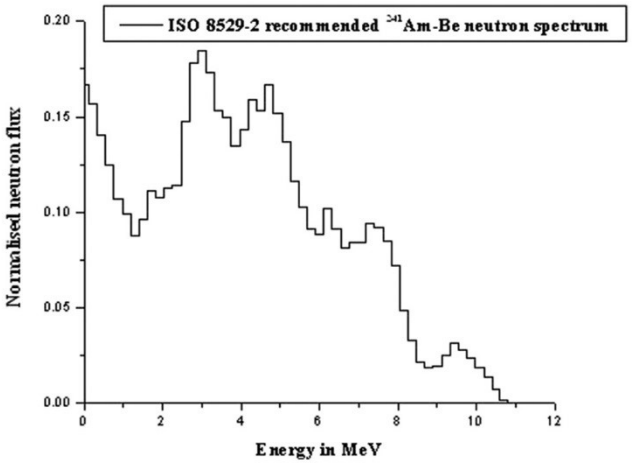

Figure 2.1: AmBe neutron spectrum from ISO 8529-2. (Technical Committee, 2016)

colors. In Figure 2.2 the graphite block is represented by the long yellow rectangle resting on the pink cylinder. In Figure 2.3 and Figure 2.4 the green rectangle denoted as structure 10 represented the table the experiment was placed on. This table was composed of wood and was 2.5 cm in height. The wood table was 58.4 cm in length and 36.8 cm in depth. Centered on top of the wood table rested a supporting plate composed of Boral. The plate is represented as structure 20, the red rectangle in both cross section figures. This Boral plate was 0.6 cm in height, 58.4 cm in length, and 34.3 cm in depth. The polyethylene cylinder was centered on top of the Boral plate. The polyethylene cylinder consisted of an outer boron doped polyethylene shell denoted as structure 34, the yellow cross section. A standard polyethylene inner cylinder was denoted as structure 33, the dark blue cross section. Inside the polyethylene cylinder was an inner air gap denoted as structure 32 and

represented by the light blue color. In the bottom of the air gap centered inside the polyethylene cylinder the AmBe neutron source denoted as structure 30 and 31 was

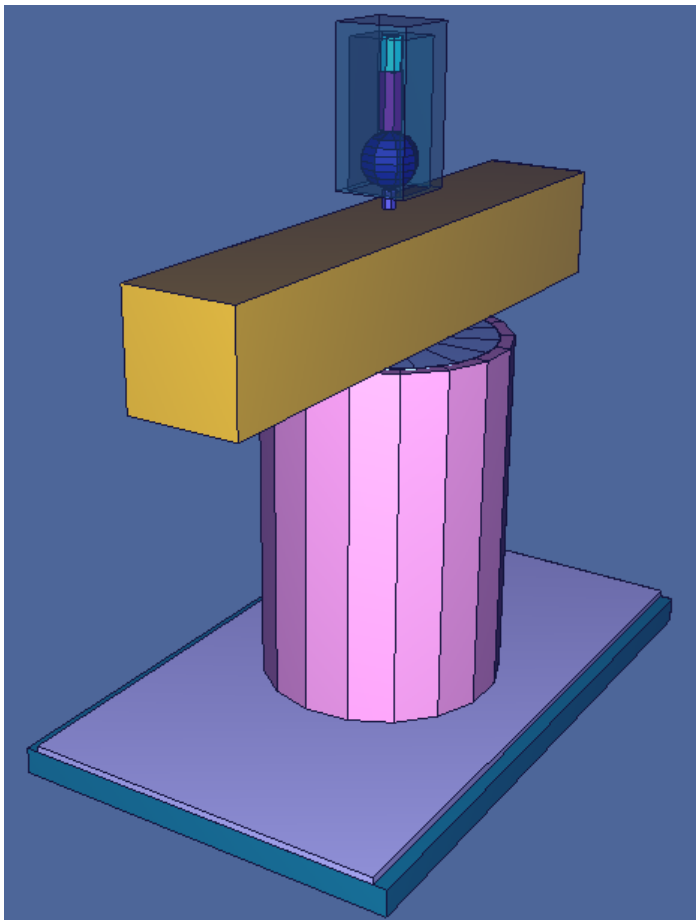

Figure 2.2: Complete simulated geometry of the standard IM1experimental configuration.

located. The AmBe neutron source is represented by the magenta and orange cross sections. The outer boron doped polyethylene shell, structure 34, was 1.3 cm thick, 33.0 cm in height, and had an outer radius of 11.4 cm from the center of the AmBe source. The inner standard polyethylene cylinder, structure 33, was 8.2 cm thick around the air gap, 33.0 cm in height, and had an outer radius 10.2 cm from the center of the AmBe source. The inner air gap, structure 32, was 3.8 cm wide and 22.3 cm in height. The AmBe source,

structure 30, was 3.2 cm in height and had a radius of 0.5 cm. The AmBe source was encapsulated by a stainless steel case, structure 31, which was 5.1 cm in height, 0.4 cm

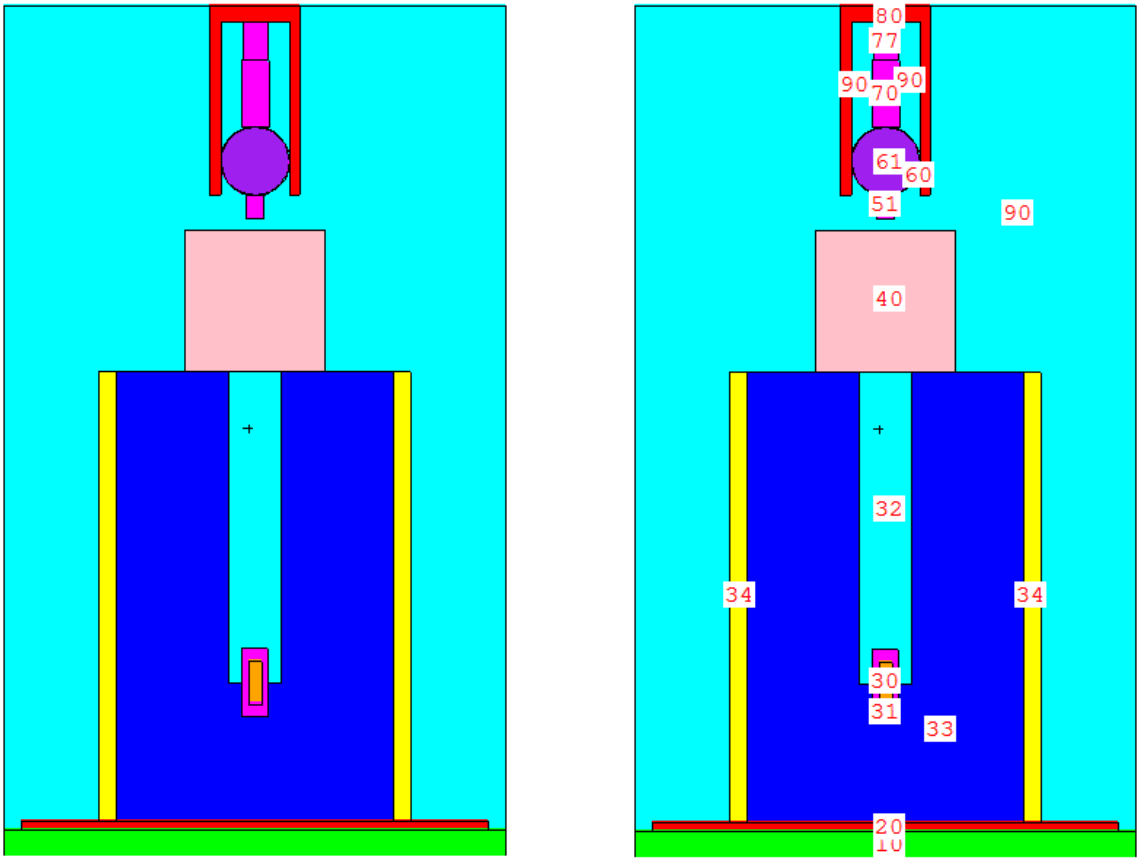

(a) (b)

Figure 2.3: XZ cross sections of the simulated IM1 experimental geometry. The figures included are of (a) the XZ cross section of the geometry and (b) the XZ cross section of the geometry with structure numbers.

thick, and had an outer radius of 0.9 cm from the center of the AmBe source. Centered on top of the polyethylene cylinder covering the air gap was the block of graphite. The block of graphite is represented as structure 40 in each cross section and is the salmon colored rectangle. The block of graphite was 10.3 cm in height, 58.4 cm in length, and 10.3 cm in

depth. Above the block of graphite, centered in line with the air gap in the polyethylene cylinder, was the BF_3 detector and the BF_3 detector shroud. The detector is made up of structures 51, 60, 61, 70, and 77 as seen in both cross sections. The bottom part of the BF_3

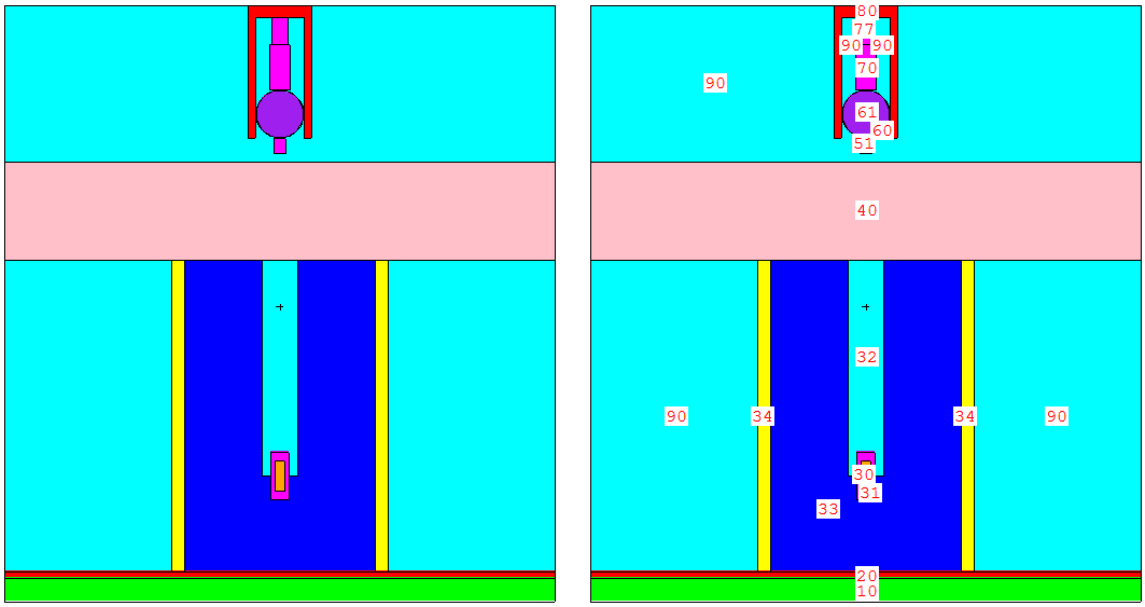

(a) (b)

Figure 2.4: YZ cross sections of the simulated IM1 experimental geometry. The figures included are of (a) the YZ cross section of the geometry and (b) the YZ cross section of the geometry with structure numbers.

detector, structure 51, is composed of stainless steel. This structure is 1.6 cm in height with 0.6 cm as the radius. The bottom end of the detector, structure 51, was 0.9 cm away from the top face of the graphite block. The spherical detector, structure 61, has a radius of 2.5 cm and was filled with BF_3 gas. The spherical detector is located 38.2 cm above the center of the AmBe source. The outer shell of the spherical detector, structure 60, has a thickness of 0.05 cm and is composed of stainless steel. Above the spherical detector region is the middle supporting structure. This middle supporting structure represented as

structure 70 is composed of stainless steel. The structure is 4.8 cm in height and 1.0 cm in radius. Above the middle supporting structure is the top structure of the BF_3 detector. This is represented as structure 77 and is composed of stainless steel as well. The top structure is 2.8 cm in height and has a radius of 0.9 cm. The BF_3 detector shroud is located around the BF_3 detector and is transparent in Figure 2.2. The detector shroud is represented as structure 80 in the cross sections. The BF_3 detector shroud is composed of Boral. The shroud is 14.0 cm in height, 0.8 cm thick on the sides, and 1.2 cm thick on the top. Air is represented in the geometry as structure 90 and is present where there is no other material. The base of the IM1 experiment including the table, Boral plate, polyethylene cylinder, and AmBe source all remained fixed throughout the simulations and experimental trials.

2.2 Year 5 Geometry

The year 5 geometry was simulated with what would be easily achieved experimentally. A graphite stack arranged with air ducts was simulated and the AmBe source was used at the end of the air duct. The same AmBe source modeled for the IM1 experiments was also used for the year 5 simulations. The air ducts where arranged in the graphite stack so that the neutrons would experience a maze that would provide them with a path of least resistance. These air ducts were meant to display the neutron streaming paths and allow for prediction of neutrons counts at the end of these paths. The preliminary geometry seen in Figure 2.5 consisted of a bottom horizontal air duct, a vertical air duct, and a top horizontal air duct all connected inside a graphite stack. This straightforward geometry was used as the basis for understanding how neutron histories evolve and will be displayed using the MCNP6 code. This preliminary geometry could also be provided

to PDT developers in order to understand computational time and results when using PDT. The geometry in Figure 2.5 was only used during simulations. This geometry was not developed experimentally although it could be configured should the need arise.

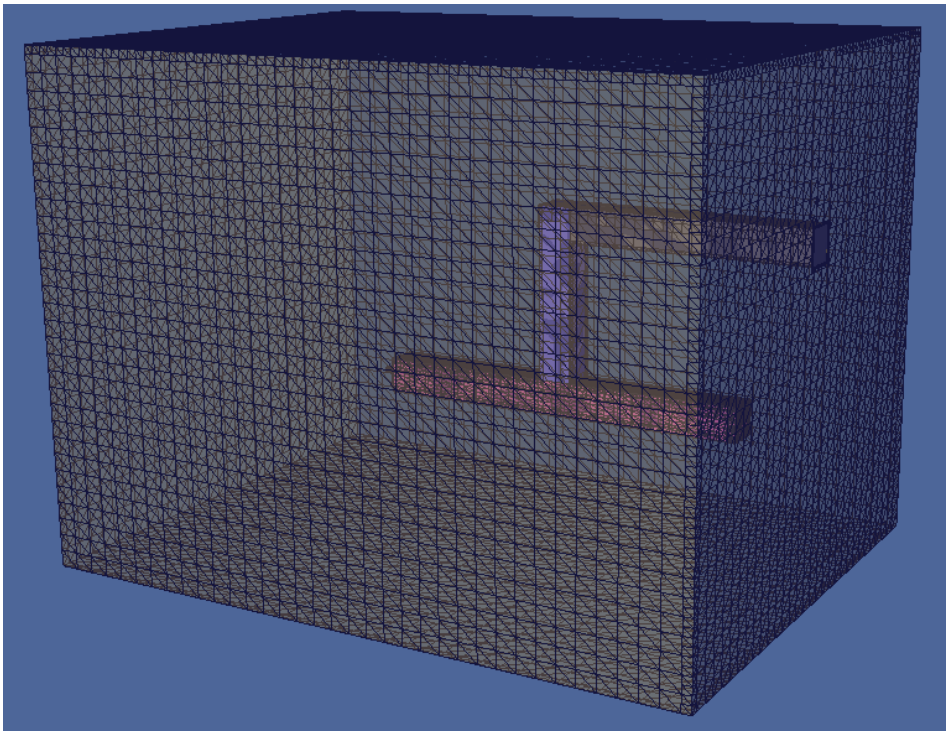

Figure 2.5: Three dimensional simulation of the preliminary year 5 geometry with air ducts encompassed in a graphite stack.

In Figure 2.5 the graphite stack is represented by the wire frame rectangle. The cross section of the year 5 geometry can be seen in Figure 2.6 below. The cylindrical AmBe source is centered on the far left face of the bottom horizontal air duct. The far left face of the bottom horizontal air duct is located 70 cm inside the graphite stack. The center of the bottom horizontal air duct is 50 cm from the bottom exterior of the graphite stack. The bottom horizontal air duct is 110 cm in length, 10 cm in height and 10 cm in depth. This air duct does not extend to the edge of the graphite stack. There is 20 cm of graphite

between the end of the bottom air duct and the exterior of the graphite stack. The vertical air duct is connected to the bottom horizontal air duct. The center of the vertical air duct

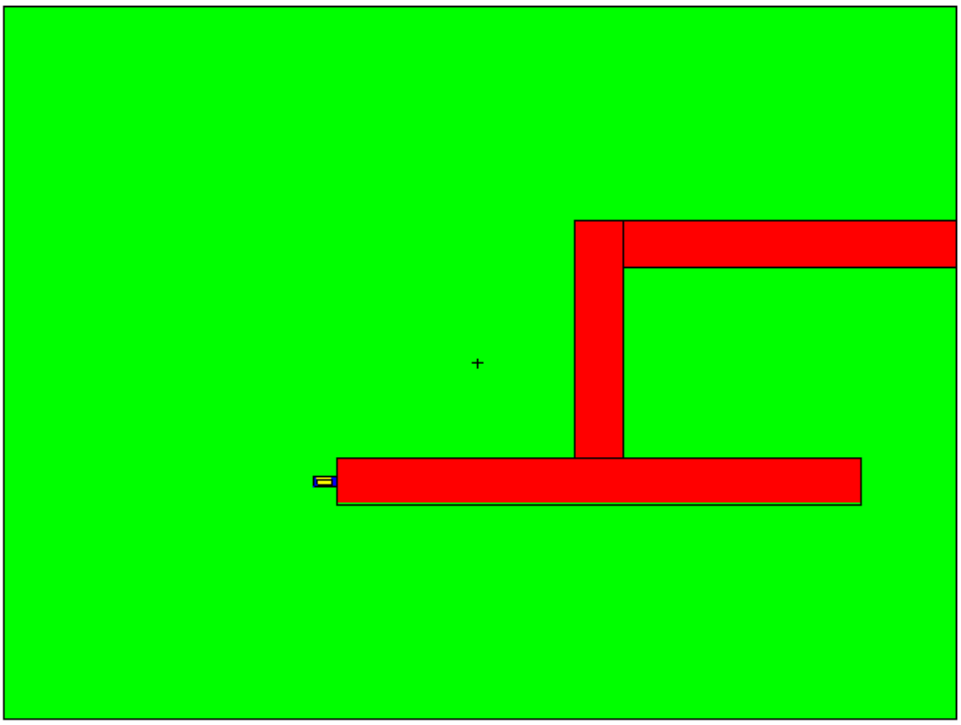

Figure 2.6: Cross section of the preliminary year 5 geometry with air ducts surrounded by a graphite stack.

is located 55 cm away from the far left face of the bottom horizontal air duct. The vertical air duct is 50 cm in height, 10 cm in width, and 10 cm in depth. The vertical air duct does not extend to the edge of the graphite stack. There is 45 cm from the top of the vertical air duct to the exterior of the graphite stack. The top horizontal air duct is connected to the vertical air duct. The top horizontal air duct is located 60 cm away from the far left face of the bottom vertical air duct. The top horizontal air duct is 70 cm in length, 10 cm in height, and 10 cm in depth. The top horizontal air duct extended to the exterior of the graphite stack. This preliminary geometry was used in order to decrease computational

time and provide a greater understanding on how the experimental set up can be configured in order to increase counting efficiency.

2.3 Neutron Generator Safety Calculation Geometry

The addition of the neutron generator introduced a new safety concern for the experimental trials. The radiation dose personnel would receive during the neutron generator operation was calculated. A drawing of the laboratory room was acquired and Figure 2.7 was created using MCNP6. This geometry only consists of the exterior walls and air making up the room. By simulating a bare geometry with only the exterior walls the dose simulated was a conservative approximation of what would be received at certain locations.

A notated cross section of the laboratory room is seen in Figure 2.8 below. Structures five, six, seven, eight, and nine, in Figure 2.8 all represent exterior walls composed of concrete. Structure five represents a concrete exterior wall which separated the laboratory room from another room being occupied. This structure was 335.3 cm in height, 508 cm in length from the front of the room to the back, and 30.5 cm in thickness. Structure six was the back exterior wall. The structure was 335.3 cm in height, 530.6 cm in length spanning the back of the room, and 45.7 cm in thickness. Structure seven was the side exterior wall. The structure was 335.3 cm in height, 508 cm in length from the front of the room to the back, and 30.5 cm in thickness. On the other side of structures six and seven soil was present due to the laboratory room being underground and on the edge of the facility. Structure eight was the exterior wall that was located adjacent to the hallway. This hallway was traveled by many employees throughout the facility. The

structure was 335.3 cm in height, 231.6 cm in length spanning from the door to the exterior wall, and 45.7 cm in thickness. Structure nine was a small part of exterior wall that was

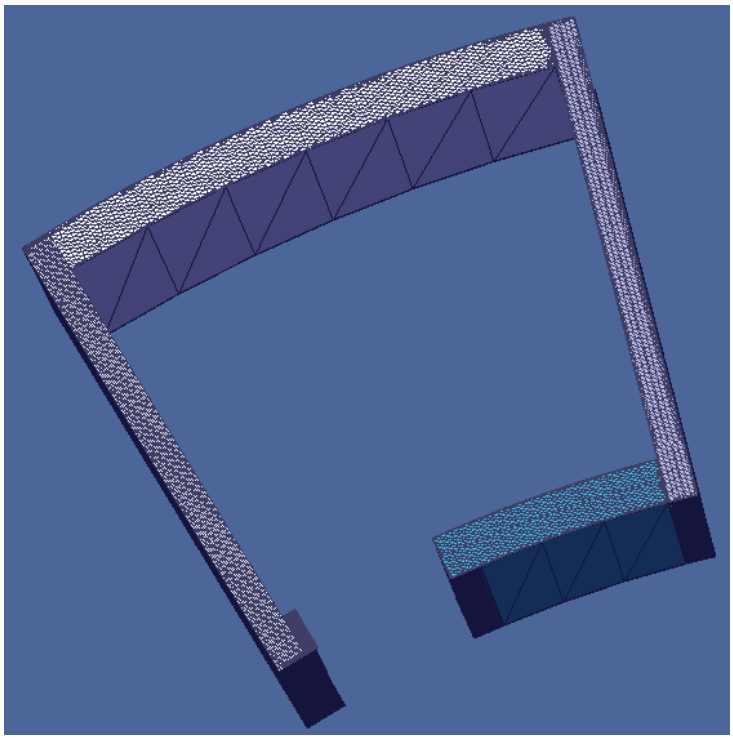

Figure 2.7: Three dimensional simulation of the laboratory room where the simulated neutron generator was located.

between region ten and structure five. Structure nine was 335.3 cm in height, 15.1 cm in length, and 45.7 cm in thickness. Region ten represented the laboratory door. For the purpose of this conservative simulation the door is assumed to be open and represented as air. The region is 335.3 cm in height, 151.3 cm in length, and 45.7 cm in thickness. Region 11 represented the entire laboratory room. For the purpose of this conservative simulation the room is approximated as simply air. Region 12 represented the air in the adjacent room. Region 13 represented the air in the hallway. The air is simulated in order to determine

how the neutrons will interact once they escape the laboratory room. Region 12 and 13 are defined so that dose measurements can be calculated at certain distances from the room.

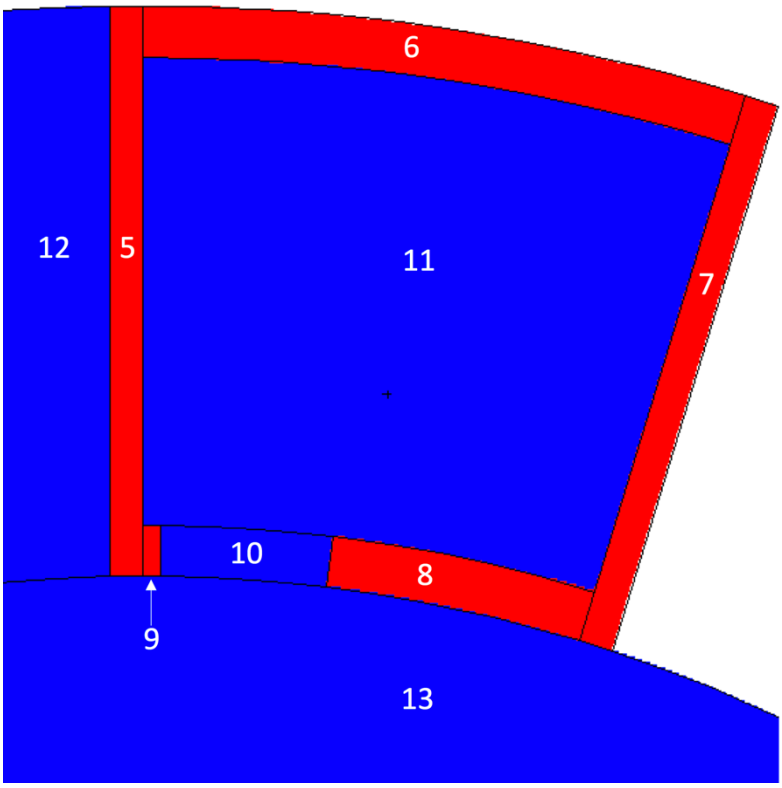

Figure 2.8: Cross section of the laboratory room where the simulated neutron generator was located.

The soil outside structures six and seven are not represented due to the fact these areas are unoccupied and the dose will not be calculated in them. This simulation was constructed without the exact placement of the neutron generator known. The geometry is made available for future refinements once more details become available.

3. RESULTS AND DISCUSSION

This section encompasses the results and analysis concluded by the MCNP6 simulations. These simulations were completed with the most current information provided at the time. Throughout this section the IM1 experiment will be discussed foremost in particular regards to the source definition used in MCNP6. Secondly, the year five experimental configuration and preliminary results will be discussed. Finally, the safety calculations will be reported.

3.1 IM1

3.1.1 AmBe Source Definition

The goal of this work was to conclude which AmBe source definition would be most appropriate for the IM1 simulation. Due to the uncertainty of the source four alternative MCNP6 definitions were explored: SOURCES 4A, SOURCES 4C, LANL, and TAMU. As expected the AmBe source spectrum provided by SOURCES 4A and 4C agreed for every data point, thus only SOURCES 4A is referenced in the results. The LANL and TAMU source each differed somewhat drastically from the others.

The SOURCES 4A source was used for many simulations and provided the baseline for many comparisons in the early stages of this project. At the time, this was known to be the most accurate representation of the AmBe source spectrum. The SOURCES 4A AmBe spectrum used can be seen in Figure 3.1 below. After immediate review of this group structure it became clear an error had been made in the implementation of the SOURCES 4A AmBe spectrum. The probability of a neutron being born between 8 MeV and 14.1 MeV was 37% based on this distribution. This was

incorrect, in fact a typical AmBe source will produce a neutron between 8 MeV and 14.2 MeV only 16% of the time. The lopsided SOURCES 4A spectrum simulated 64.7

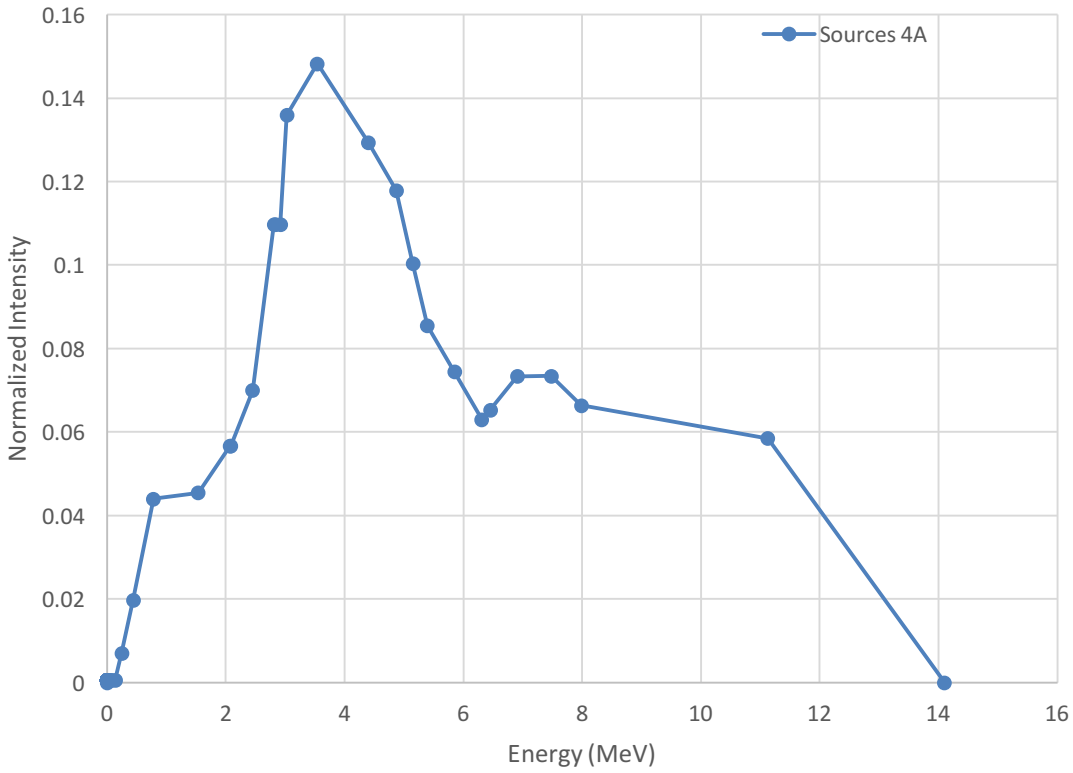

Figure 3.1: Original SOURCES 4A 99 group AmBe source spectrum.

absorptions per second in the BF_3 detector when no graphite blocks were present. This source definition also simulated 14.7 absorptions per second in the BF_3 detector when the graphite was in the standard position. When comparing the ratio of these results with the ratio of the PDT results there was agreement. However, the experimental results did not align. It was this discrepancy that initiated the in-depth review of the MCNP6 input deck.

The large probability of high energy neutrons being born was then discovered from Figure 3.1.

Through some internal investigation it was determined the python script which formulated a 99 group source definition from the 48 group SOURCES 4A definition had an error in it. This error would not treat the energy distribution above 10 MeV correctly. The 99 group source definition was defined coarsely above 8 MeV only two data points where being inputted. There was an energy bin midpoint at 11.1 MeV and a midpoint of 14.1 MeV. Due to the coarse treatment of the higher neutron energy bins this caused the error in the python script to be compounded.

Once the python script was corrected a new 99 group source definition was formed from the SOURCES 4A data. As can be seen in Figure 3.2 the probability of a neutron being born between 8 MeV and 14.2 MeV from the AmBe source was significantly decreased. This correction allowed for a 16% probability that a neutron would be born in the above range as is typically expected for an AmBe source. This new source definition was then inputted into the MCNP6 input deck and the simulations were completed. By changing the probability of a high energy neutron being born the absorptions per second each changed. When the IM1 simulation was completed with no graphite block present the simulation recorded 71.0 absorptions per second in the BF_3 detector. When the graphite bar was placed in the standard postion the simulation recorded 15.7 absorptions per second in the BF_3 detector. This increase in recorded counts drew immediate attention that the source defintion may have been the cause of why there was deviation between simulated and experiemental results. However, this updated ratio of the counts still did not take into

account other errors that may be present in the source defintion. The ratio of the two simulations (air and graphite) resulted in about 0.36% error from experimental results. It was determined the source defintion needed to be investigated further.

In order to further explore the SOURCES 4A spectrum a 115 energy group source definition was derived. In Figure 3.3 the shape of the 115 group spectrum is nearly identical to Figure 3.2. The 115 group spectrum deviates slightly at 1 MeV and at 3.5 MeV from the 99 group structure. This spectrum was designed in order to ensure the high energy

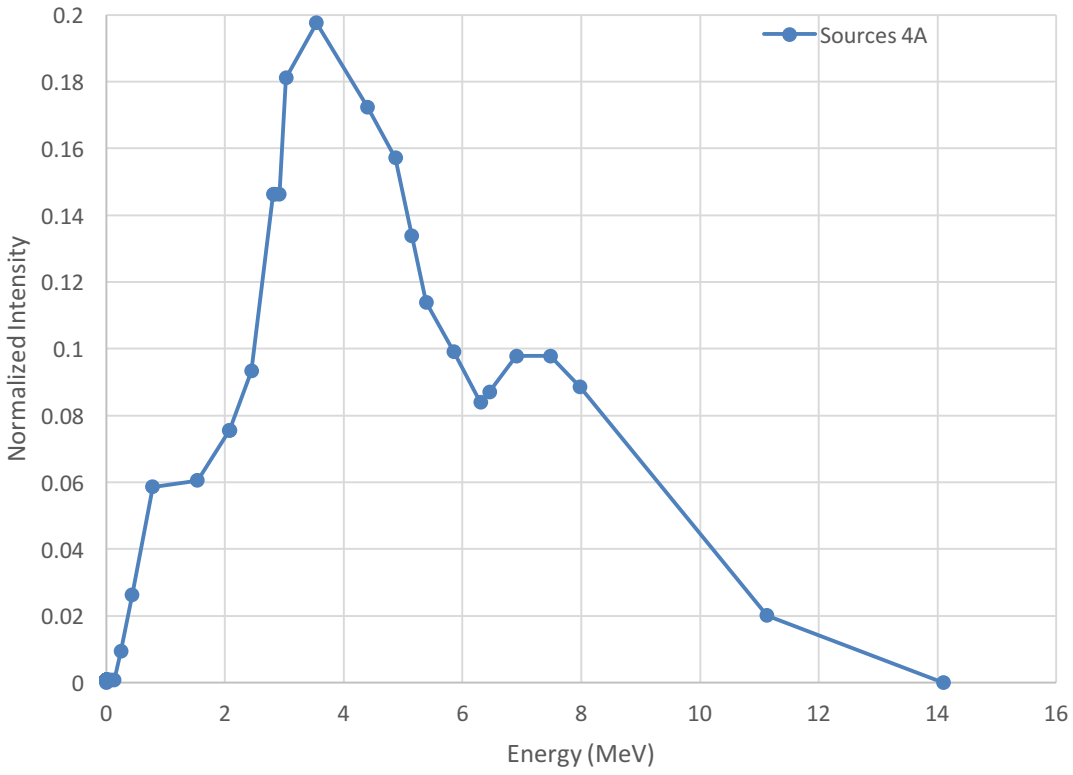

Figure 3.2: Corrected SOURCES 4A 99 group AmBe source spectrum.

neutrons where being treated correctly as well as provide additional discrimination throughout the energy ranges. The probability a neutron will be born with an energy

between 8 MeV and 14.2 MeV is 16.3% for the 115 energy group SOURCES 4A spectrum. For this source definition there is a 3.4% probability a neutron will be born in the energy range 0 MeV to 1.3 MeV. The 115 group structure was used in the IM1 simulations with a graphite block present and without one. The air only simulation yielded 71.5 absorptions

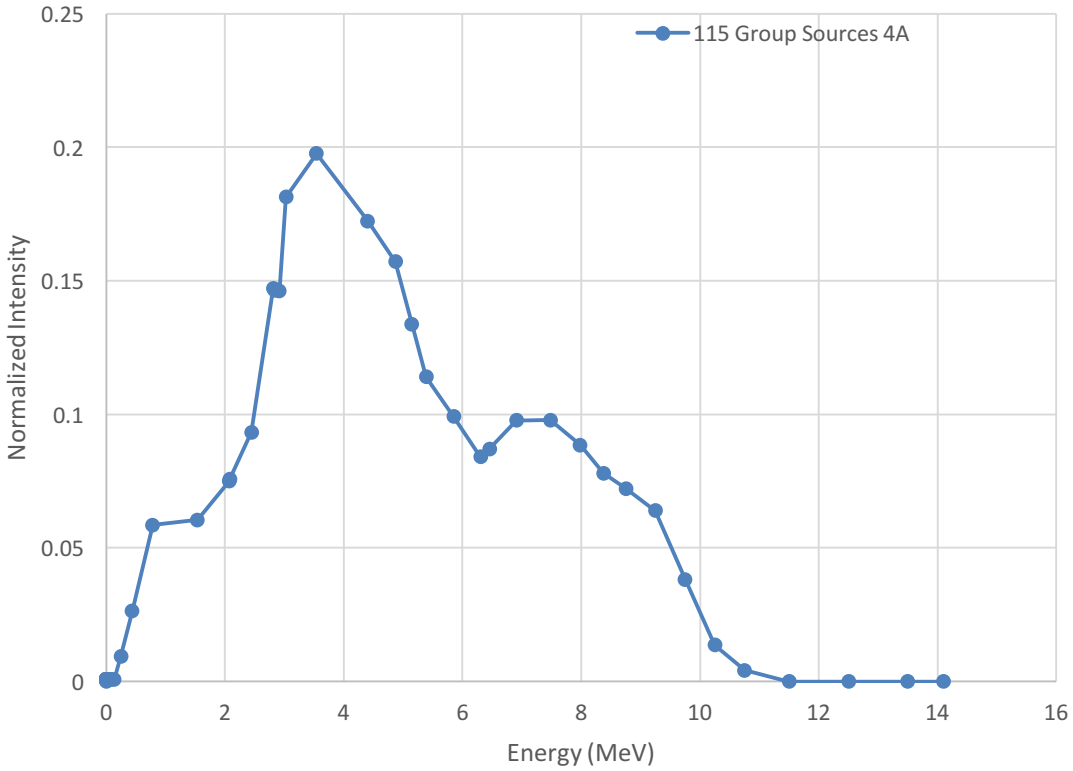

Figure 3.3: 115 group SOURCES 4A AmBe source spectrum.

per second in the BF_3 detector. After the graphite block was placed in the simulation the absorptions per second decreased to 15.9 in the detector volume. This group structure was mainly used as a baseline for future PDT comparisons.

The next source definition that was explored was provided by Dr. Tim Goorley of Los Alamos National Laboratory. The LANL source definition in Figure 3.4 is a much more structured source spectrum then previously analyzed. The spectrum is full of peaks and valleys meant to resemble ISO 8529-2 found in Figure 2.1 above as closely as possible. It becomes immediately apparent that the LANL spectrum uses many more groups in the higher energy range then the 99 group structure extrapolated from the

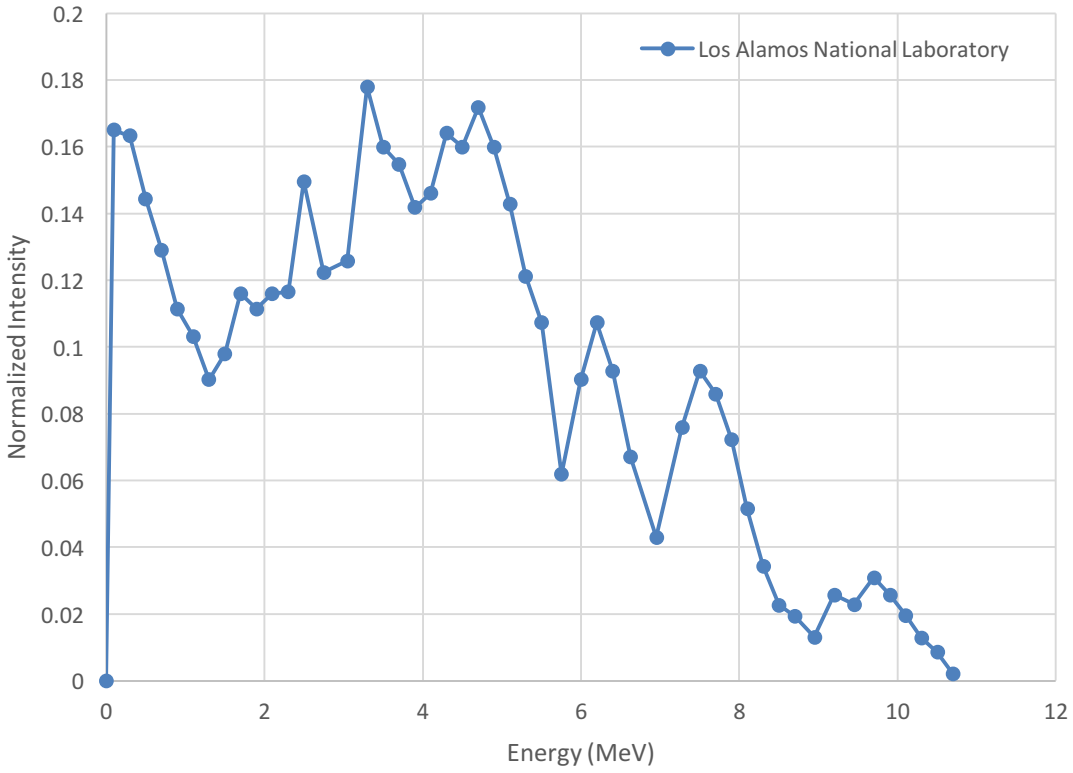

Figure 3.4: Los Alamos National Laboratory AmBe neutron source spectrum.

SOURCES 4A data. The probability a neutron will be born having an energy between 8 MeV and 14.2 MeV is 9.3% for the LANL spectrum. This is nearly half the probability of the SOURCES 4A spectrum. This decrease in probability is due to the LANL source

definition having simulated a larger probability of low energy neutrons in the range 0 MeV to 1.3 MeV. For the LANL source definition there is a 16.3% chance a neutron will be born in the energy range 0 MeV to 1.3 MeV. As opposed to the SOURCES 4A spectrum where there is a 6.6% probability a neutron will be born in the same energy range. The IM1 simulation was completed with no graphite bar present yielding a result of 83.0 absorptions per second in the detector volume. The IM1 simulation was then completed with the graphite bar in the standard position resulting in 16.9 absorptions per second in the detector volume.

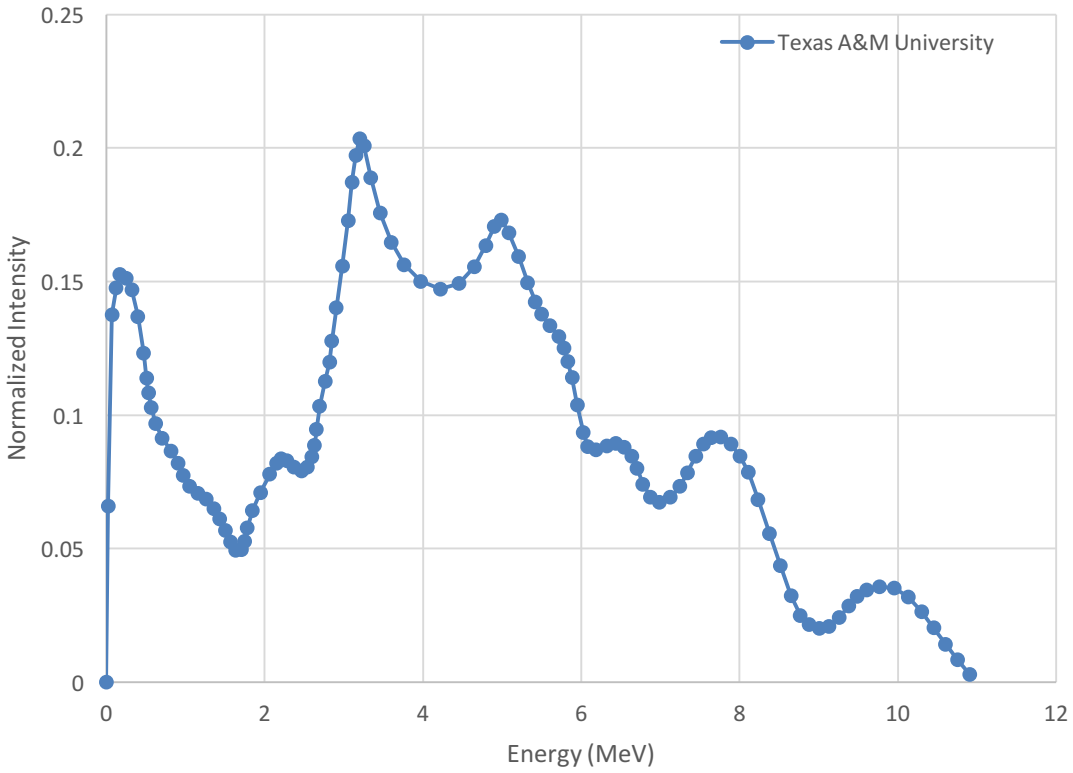

Figure 3.5: Texas A&M University AmBe neutron source spectrum.

The final AmBe spectrum analyzed was provided by Dr. Sunil S. Chirayath of Texas A&M University. This spectrum was provided as a supplement in a graduate MCNP course taught at Texas A&M, NUEN 630. The AmBe source spectrum represented in Figure 3.5 attempts to represent a combination of both the SOURCES 4A spectrum as well as the LANL spectrum. In the lower energy ranges the TAMU spectrum is representative of the LANL spectrum. However, at 0.91 MeV the spectrum shifts to align with the SOURCES 4A spectrum. The TAMU spectrum then converges on the same shape as the LANL spectrum from 3.46 MeV to 11 MeV with slight deviations. This spectrum was constructed using 114 different energy groups. The probability a neutron will be born having an energy between 8 MeV and 14.2 MeV is 11.05% for the TAMU spectrum. For the TAMU source definition there is a 13.6% chance a neutron will be born in the energy range 0 MeV to 1.3 MeV.

Table 3.1: Ratio of the simulation results for the IM1 experiment with a graphite bar present to the IM1 experiment without a graphite bar present (Air Case).

Source Definition	Experimental Set Up	Absorptions per a Second	RSE	Ratio
Original Sources 4A	Graphite	14.7	0.0025	0.227
	Air	64.7	0.0011	
Corrected Sources 4A	Graphite	15.7	0.0025	0.221
	Air	71.0	0.0011	
115 Group Sources 4A	Graphite	15.9	0.0025	0.222
	Air	71.5	0.0011	
LANL	Graphite	16.9	0.0024	0.204
	Air	83.0	0.0010	
TAMU	Graphite	16.5	0.0024	0.210
	Air	78.7	0.0010	

The TAMU spectrum was inserted into the IM1 input deck and the simulation was completed yielding 78.7 absorptions per second in the detector volume when there was no graphite bar present. With the presence of a graphite bar in the IM1 simulation 16.5

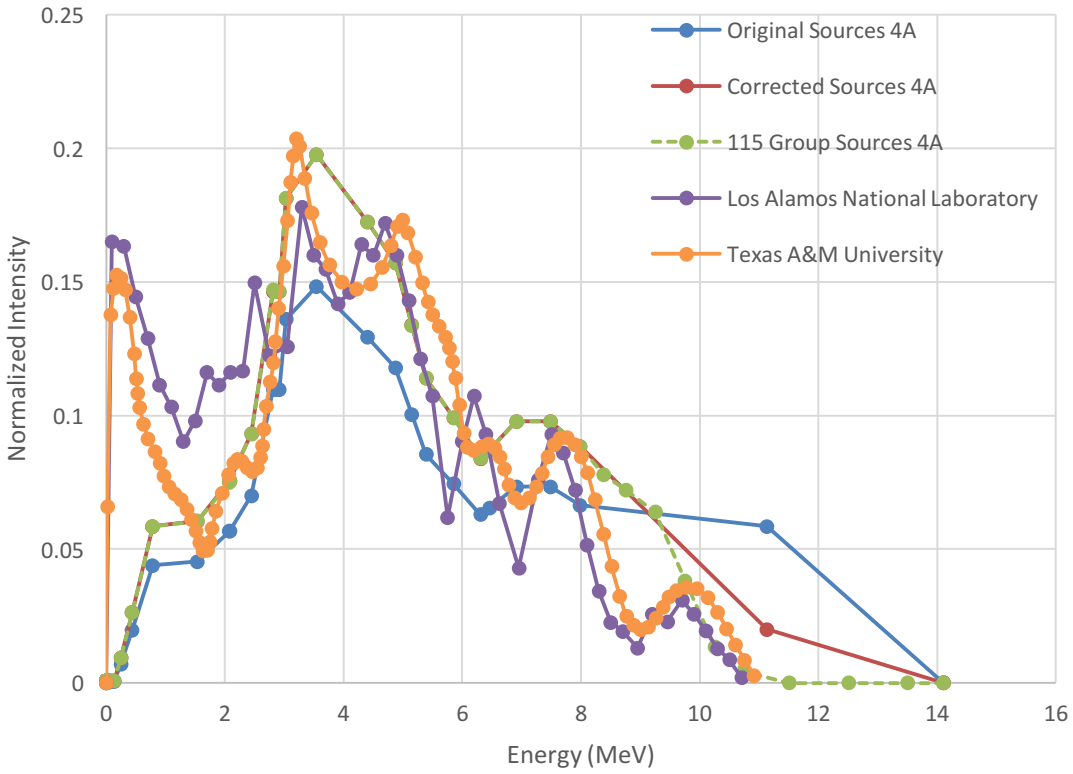

Figure 3.6: Combination of all source definitions analyzed throughout this project.

absorptions per second where recorded in the detector region. These numbers are expected as this spectrum is a combination of both the corrected SOURCES 4A and LANL spectrums. In Table 3.1 above the ratio of the graphite simulation to the air simulation (no graphite present) is reported for each source definition.

In order to best compare these five source spectra Figure 3.6 shows each one plotted together such that the area under each individual curve is normalized to one. The original SOURCES 4A definition should immediately be discarded as this had an error in the higher energy ranges. The other four curves each follow a similar pattern with their own unique properties. The LANL and Texas A&M University spectrum should also be rejected for the purpose of this project. The origination of each of those spectra could not be validated.

3.1.2 Graphite Block Experiments

The goal of this work was to create multiple MCNP6 input decks that could be used to further calibrate the IM1 model. Excluding the standard IM1 experimental configuration, five different placements of graphite blocks and the BF_3 detector were constructed. These specific geometries were created in MCNP6 in order to supplement the calibration process experimentally, as well as in PDT. The standard IM1 graphite simulation geometry is thoroughly explained in Section 2.1. For all of the different specific configurations the base of the IM1 experiment remained constant. This consisted of a base wood table. Centered on top of the wood table was a Boral plate. Centered on the Boral plate was a polyethylene cylinder, with an outer Boron doped shell and an inner air gap. The AmBe neutron source rested in the bottom of the air gap centered in the polyethylene cylinder.

The standard IM1 geometry displayed in Figure 3.7 was constructed using one graphite block centered on the polyethylene cylinder such that the air gap was completely covered. The BF_3 detector apparatus was located above the graphite block. The graphite

block was 58.42 cm long with respect to the face the detector was perpendicular to. In addition, the graphite was 10.3 cm in depth and 10.3 cm tall. The detector was located 0.9 cm away from the nearest graphite face and directly in line with the air gap located inside the polyethylene cylinder. A more thorough description of this simulation can be found in Section 2.1 IM1 Geometry above. The simulation estimated 13.4 absorptions per second

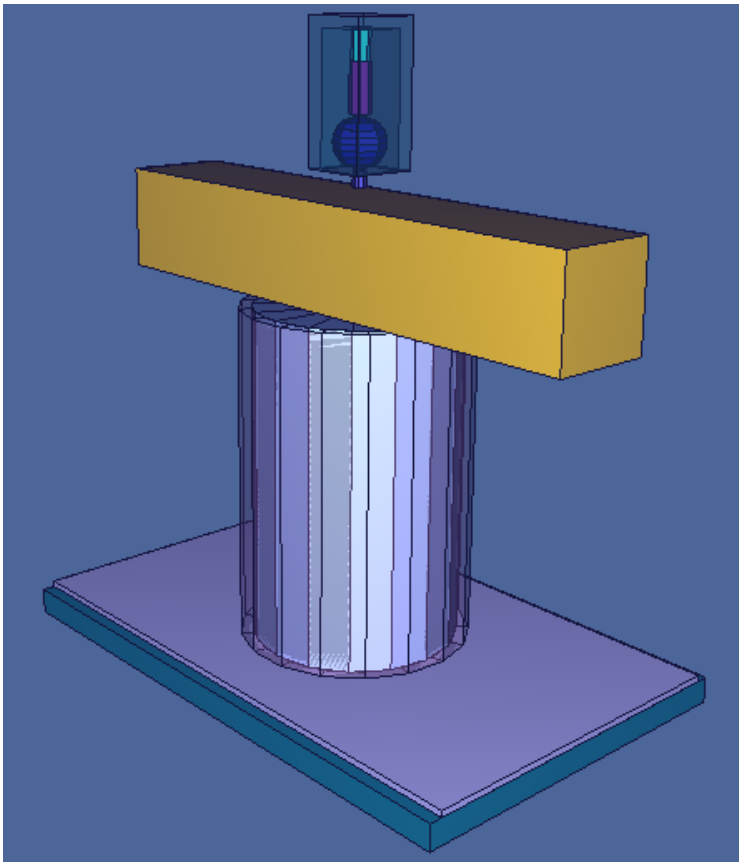

Figure 3.7: Standard IM1 geometry used as a baseline for alternative configurations.

with a relative standard error of 0.0027 in the BF3 detector region. The simulation was also completed with the graphite block removed and replaced with air. This configuration is known as the air case. The air results estimated 63.1 absorptions per second with a

relative standard error of 0.0012 in the BF3 detector region. The increase in absorptions per second was as expected, with the removal of the graphite block the neutrons had an unobstructed streaming path from the AmBe source, up the air gap, straight to the detector region.

The first alternative geometry shown in Figure 3.8 consisted of three graphite blocks stacked side by side across the y-axis of the polyethylene cylinder base. These three blocks covered the air channel on top the polyethylene cylinder. The BF_3 detector apparatus was lowered and rotated to be mid-plane with the graphite blocks. The yellow rectangle in Figure 3.8 represents the three graphite blocks stacked overtop the

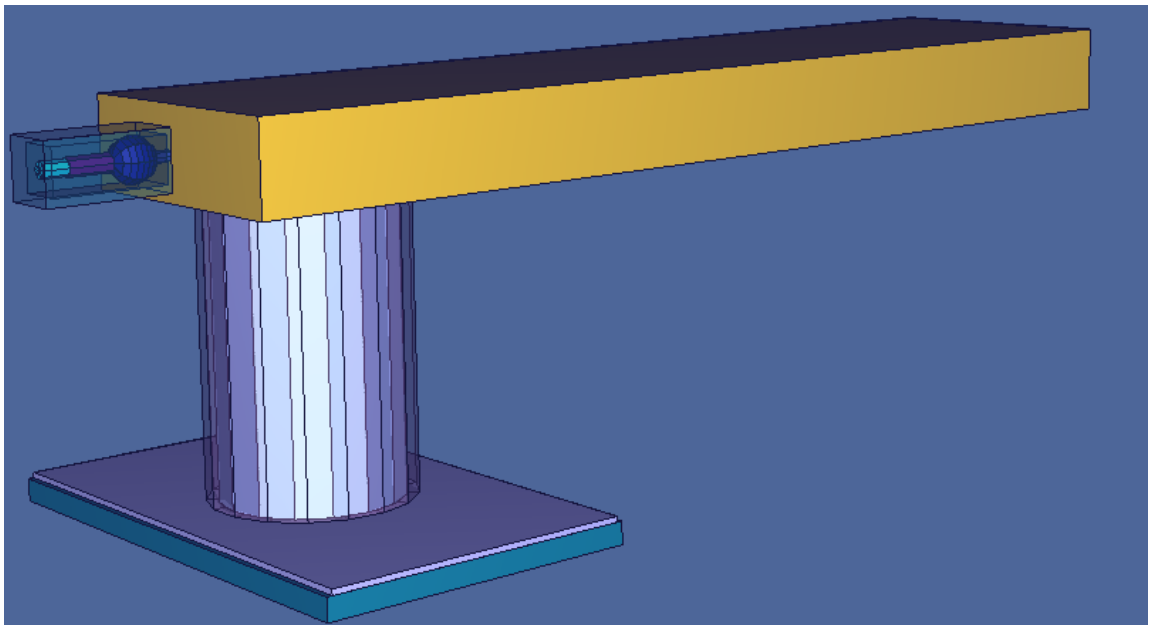

Figure 3.8: Alternative configuration one using an offset graphite block placement.

polyethylene cylinder. In this configuration the BF_3 detector would only record counts from neutrons that stream up to the graphite block and then scattered to the left. The detector apparatus was surrounded by Boral plating only allowing neutrons to enter from

the opening which is aligned facing the end of the graphite block. The graphite block is 30.9 cm wide where the detector is located. The graphite block is 127 cm long and 10.3 cm tall. The bottom of the detector apparatus is 0.9 cm away from the graphite and is 16.1 cm away from the center of the air gap in the polyethylene cylinder.

The second alternative show in Figure 3.9 consisted of three graphite blocks placed on top of the polyethylene cylinder as in Figure 3.8, however this configuration centered the total length of the graphite on the center of the air gap. Therefore, there is an equal amount of graphite on each side of the polyethylene cylinder. The detector apparatus is

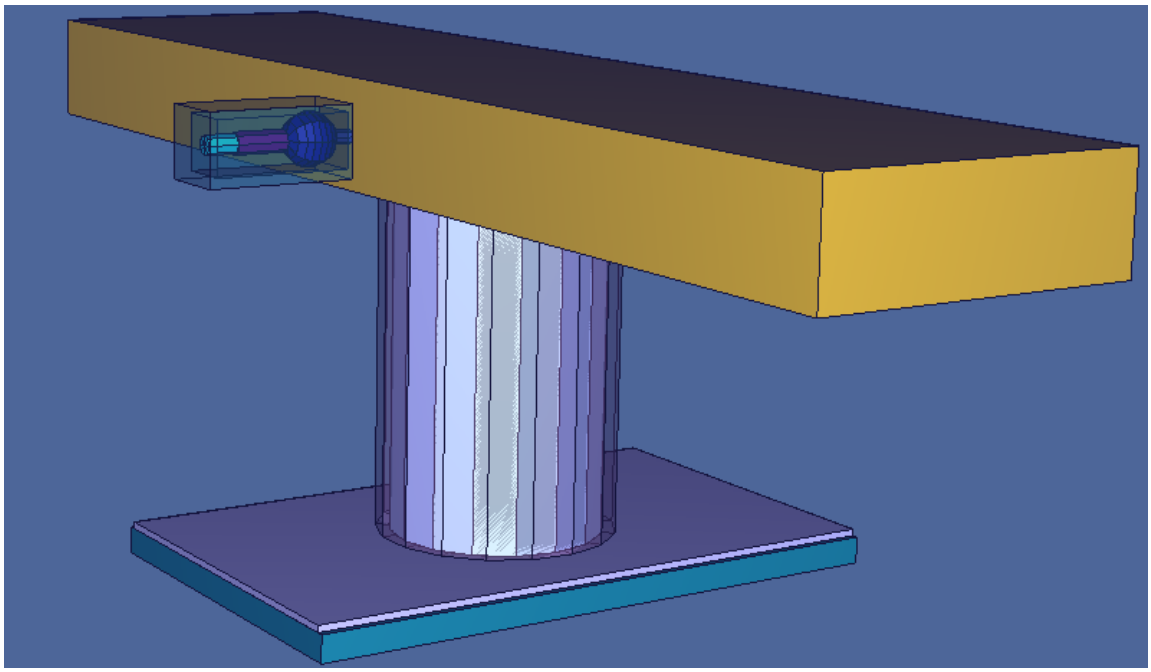

Figure 3.9: Alternative configuration two utilizing equal spacing of three graphite blocks along the y-axis, with the detector centered on the side of the graphite.

again lowered and rotated such that is located on the center of the long face of the graphite. This configuration allows for different neutron streaming paths to enter the detector volume when compared to the first alternative configuration, due to the graphite and

detector placement. The graphite is 127 cm long on the plane the detector faces. The graphite block is 30.9 cm in depth and 10.3 cm tall. The detector is centered mid-plane on the graphite block and is 0.9 cm away from the nearest graphite face and 16.4 cm from the center of the air gap in the polyethylene cylinder.

The third alternative configuration show in Figure 3.10 consisted of three graphite blocks spaced across of the polyethylene cylinder as in Figure 3.9 previously. The detector apparatus remained vertical in its standard configuration. This alternative configuration is

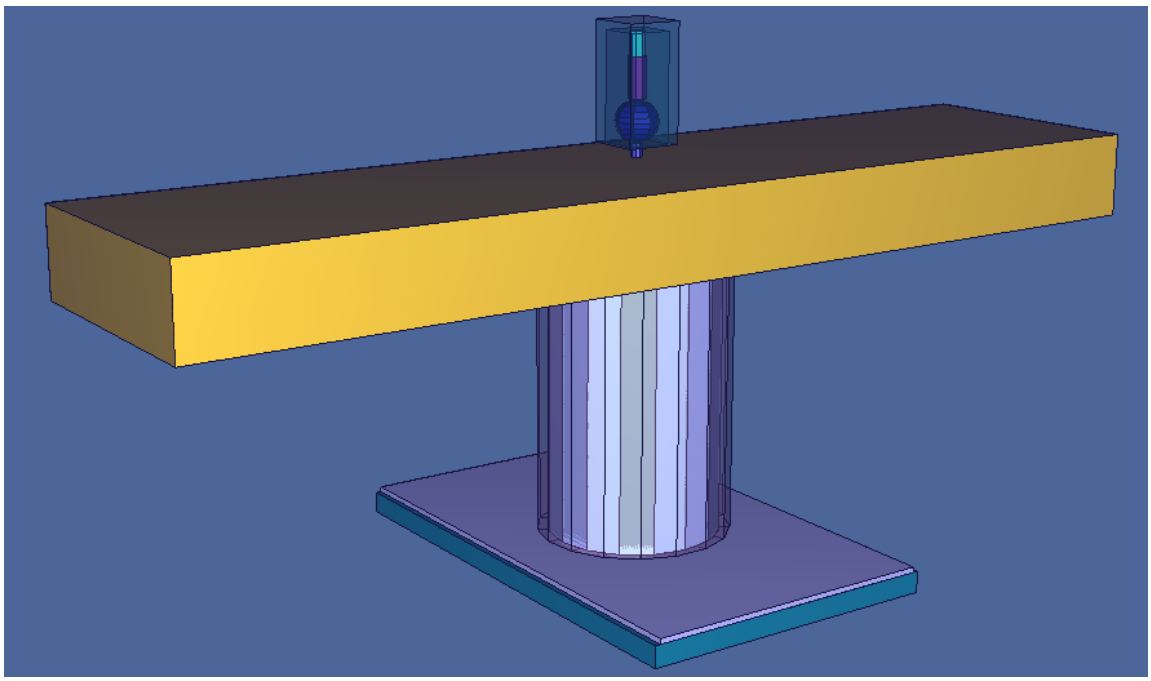

Figure 3.10: Alternative configuration three utilizing equal spacing of three graphite blocks along the y-axis, with the detector above the graphite.

slightly different from the standard setup in that there were three blocks of graphite instead of one. The BF_3 detector is centered on the graphite block as well as centered in relation to the air gap in the polyethylene cylinder. This configuration would expect to exhibit similar absorptions in the detector as the standard IM1 setup. The addition of two graphite

blocks will allow the neutrons more surface area to scatter and enter the detector region. The graphite block is 127 cm long across the face the detector is perpendicular to. The graphite block is 30.9 cm in depth and 10.3 cm tall. The detector is located 0.9 cm away from the nearest graphite face and directly in line with the center of the polyethylene cylinder air gap.

The fourth alternative configuration shown in Figure 3.11 was constructed with two graphite blocks stacked on top of each other, as opposed to beside each other. These blocks are centered above the polyethylene cylinder. The detector apparatus had to be

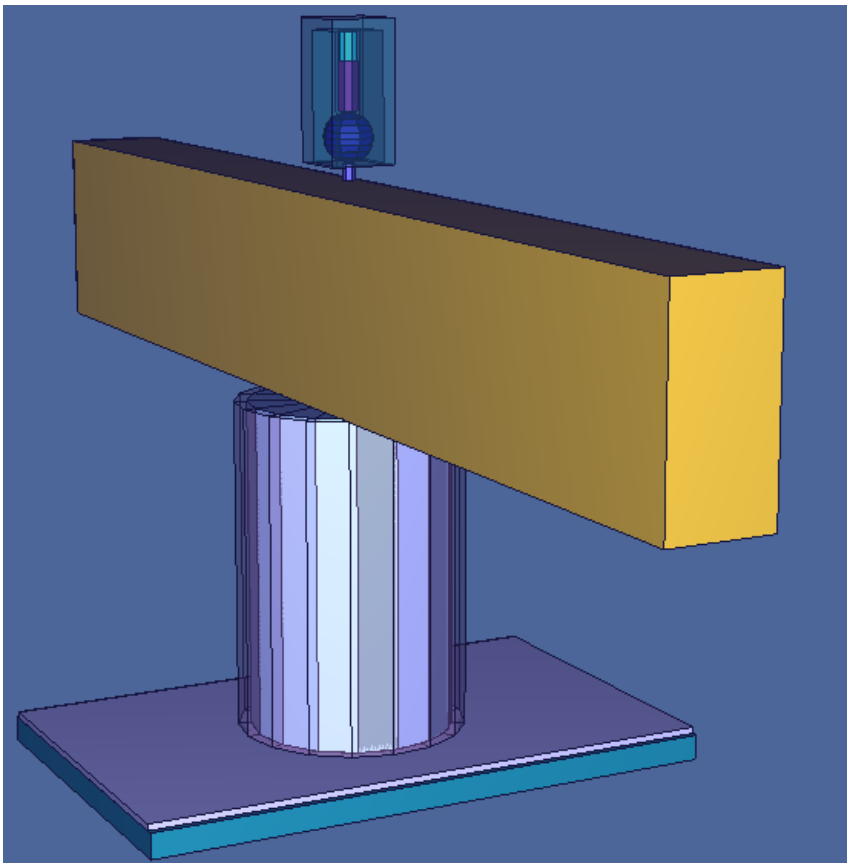

Figure 3.11: Alternative configuration four utilizing two stacked graphite blocks along the z-axis, with the detector above the graphite.

raised in the z-direction to account for the additional height of the stacked graphite. This configuration should yield similar results to the standard IM1 setup. The additional graphite block will increase the amount of surface area the neutrons can scatter off of. The graphite block was 127 cm long in regards to the face perpendicular to the detector. The graphite was 10.3 cm in depth and 20.6 cm tall. The detector is centered on the graphite block in line with air gap in the polyethylene cylinder and is 0.9 cm away from the nearest graphite face.

The fifth alternative configuration displayed in Figure 3.12 is a combination of Figure 3.9 (alternative configuration two) and Figure 3.10 (alternative configuration three)

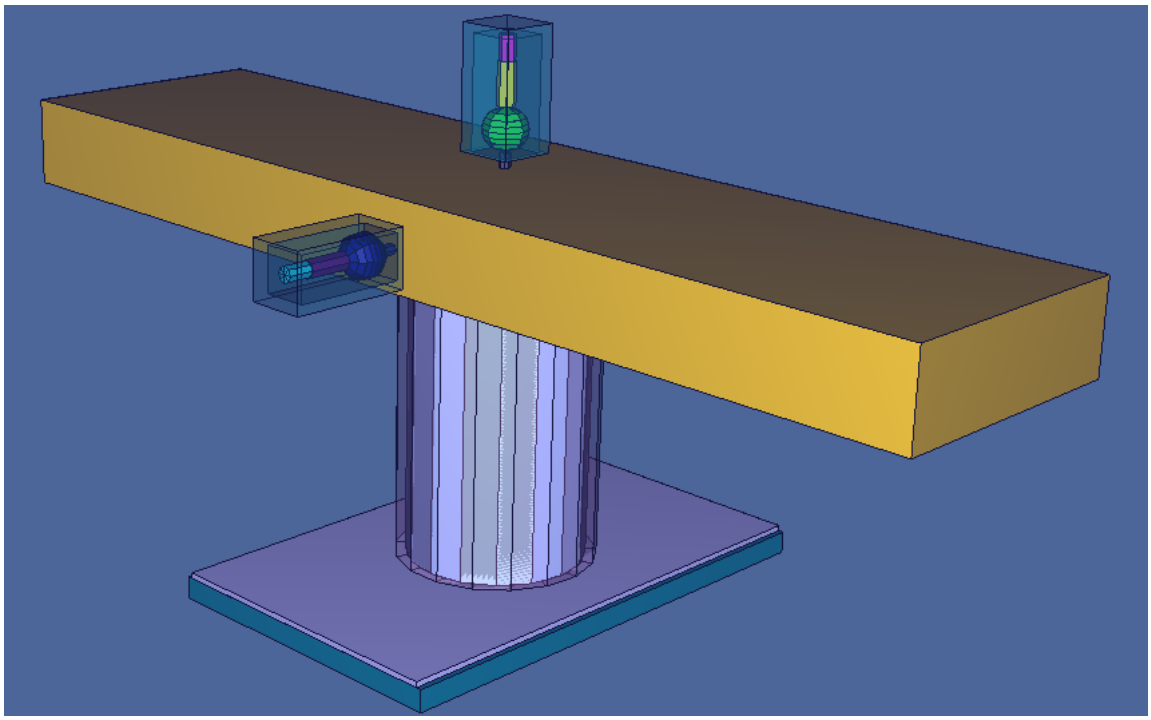

Figure 3.12: Alternative configuration five utilizing equal spacing of three graphite blocks along the y-axis. One detector is located above the graphite and one detector is on the side of the graphite block.

above. This final configuration was created in order to limit the large amount of simulations required to use these experimental setups. The addition of a second identical detector apparatus in the simulation allowed for this combination of input decks. This was able to reduce the number of run sets required in order to compare these simulations with experimental results. These MCNP6 input decks are transformed into PDT readable formats and therefore allowing for alternative configuration five to be used instead of alternative configuration two and three separately. This combination greatly aids in preserving computational time.

The different graphite geometries created aided in the advancement of the IM1 experiment. The standard configuration along with all five alternative configurations allow for PDT to perform simulations and compare the results with that of MCNP6 and experimentally. Should further IM1 characterization be needed the alternative geometries where made available for use.

3.1.3 Boric Acid Experiments

The goal of this work was to produce an MCNP6 geometry that represented the boric acid experiments. The boric acid experiments provided a baseline in order to examine what would happen to the absorptions per second recorded by the BF_3 detector given a known impurity. In these experiments the known impurity was the boron concentration in the solution. This impurity was molded by changing the boric acid concentration present in the solution for multiple scenarios. In order to increase efficiency and save time the boric acid experimental configuration is very similar to Figure 3.7 the standard IM1 experimental setup. The base as previously described in Section 2.1 IM1

Geometry remained constant for these simulations. The only addition was a beaker filled with certain concentrations of boric acid.

The acrylic beaker was placed on top of the polyethylene cylinder as represented in Figure 3.13 with the air gap fully covered. An XZ cross section of the simulated geometry is presented in Figure 3.14 below. The dimensions of the acrylic beaker experimentally used were recorded. The visual cross section of the acrylic beaker in Figure 3.14 is represented by the grey rectangles. The beaker was 0.6 cm thick at the base and had an outer radius of 5 cm. The outer beaker walls were 0.6 cm thick and the beaker was

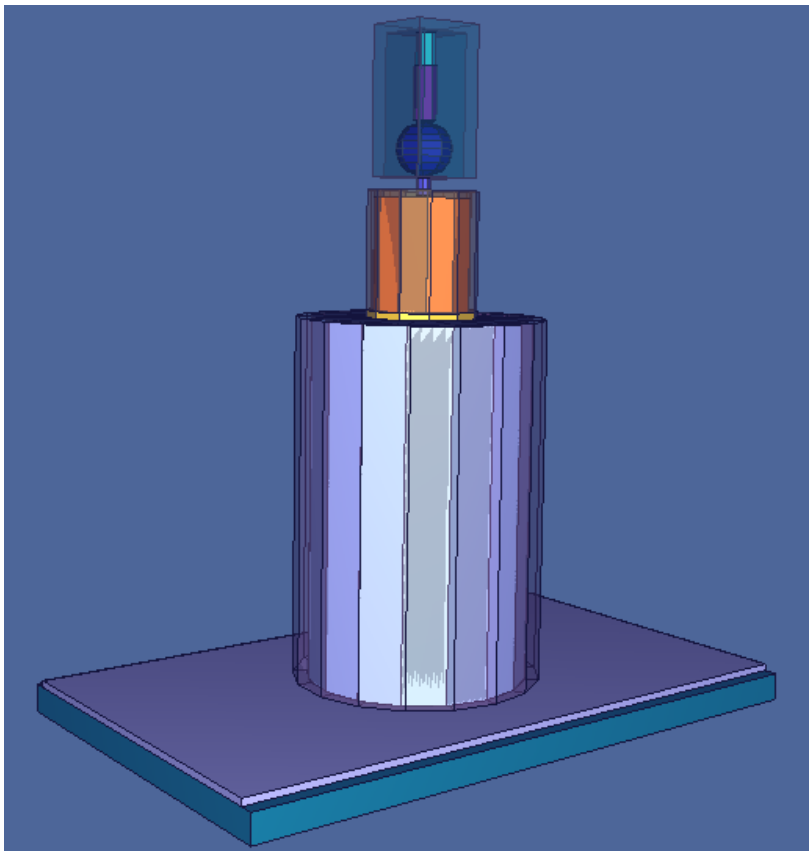

Figure 3.13: Boric acid simulated geometry of experimental configuration.

11.4 cm tall. The visual cross section of the boric acid solution in Figure 3.14 is represented by the white box encompassed by the grey rectangles. The height of the boric acid solution inside the beaker was 10.1 cm and the volume of boric acid was 630.6 cm^3 inside the beaker. The height and volume of solution in the acrylic beaker remained constant for each different concentration of boric acid. The standard BF_3 detector apparatus was used for the boric acid experiments. The detector was located 0.2 cm away from the boric acid solution and was placed slightly inside the acrylic beaker. The detector was centered with respect to the beaker and the air gap located inside the polyethylene cylinder.

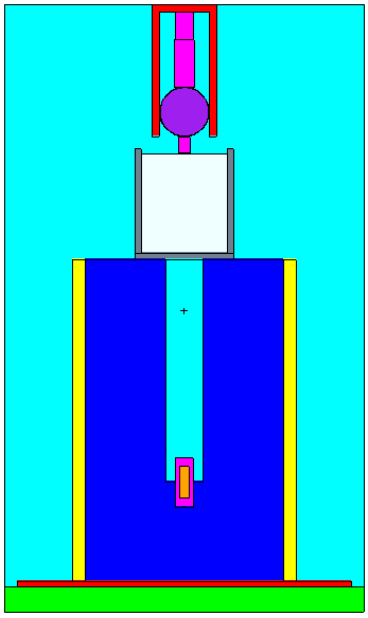

Figure 3.14: Boric acid XZ cross section of the simulated experimental geometry.

The simulation was completed using thirteen different boric acid concentrations ranging from 0 ppm of boric acid up to 600 ppm of boric acid. The results of these simulations are provided in Table 3.2 below. Only water was present in the beaker for the

Table 3.2: Boric acid simulation results of absorptions per second recorded in the BF_3 detector region.

Boric Acid Concentration (ppm)	Absorptions/Second	Absolute Error
0	6.288	0.025
50	6.110	0.024
100	5.932	0.024
150	5.758	0.024
200	5.597	0.024
250	5.433	0.023
300	5.288	0.023
350	5.157	0.023
400	5.030	0.023
450	4.917	0.022
500	4.794	0.022
550	4.679	0.022
600	4.576	0.022

0 ppm boric acid scenario. As the concentration of boric acid in the solution is increased the absorptions per second simulated in the detector region decreased as expected. This is due to the additional atoms of boron, which increased the overall absorption cross section the neutrons interacted with. From Figure 3.15 it becomes apparent as the boric acid concentration is increased by 50 ppm, with each additional simulation, the absorptions per second follow a distinct exponential trend.

Equation 3.1 was developed in order to predict the absorptions per second simulated in the detector. This equation may be used as a means to predict the absorptions per second expected in the PDT simulations and future experimental results.

$$y = 6.2435e^{-5\times10^{-4}\times b} \tag{3.1}$$

In Equation 3.1, b is the boric acid concentration in parts per million and y is the predicted absorptions per second in the detector region. In order to decrease the statistical error in these simulations four billion particle histories were created. These results along with

experimental and PDT results provided validation on how the detector should react given certain impurities.

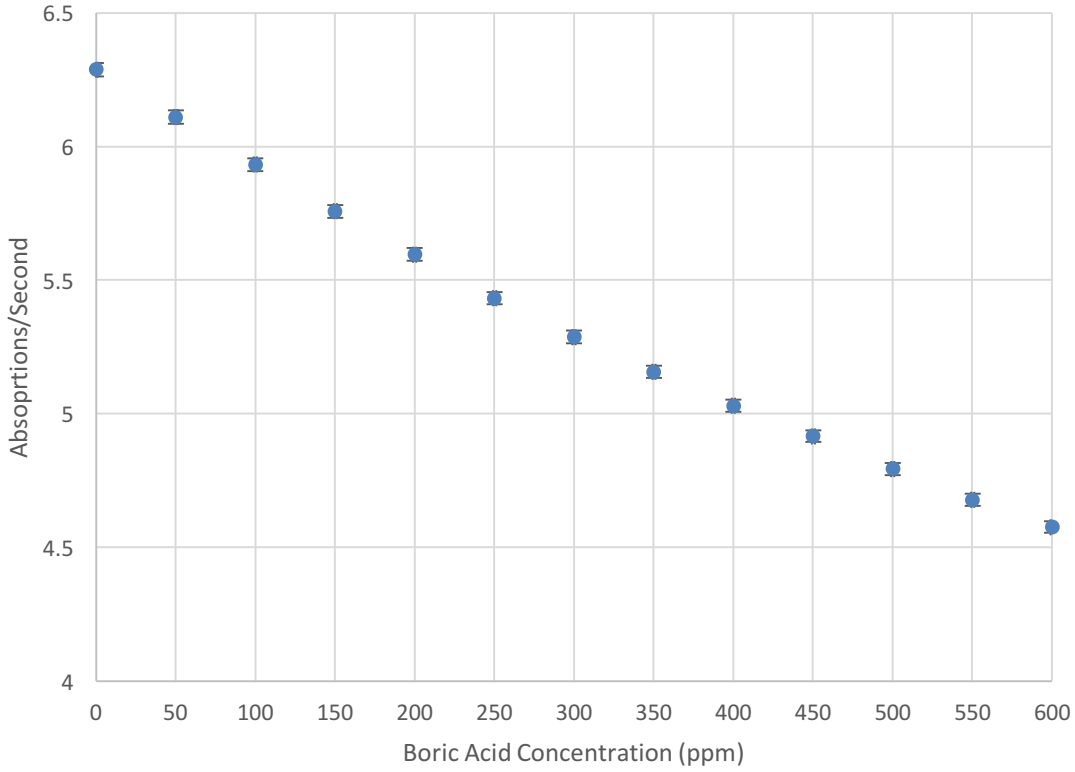

Figure 3.15: Boric acid simulation results of absorptions per second as a function of boric acid concentration in ppm.

3.1.4 Polyethylene Experimental Enclosure

The goal of this work was to modify the standard IM1 geometry with the addition of a borated polyethylene box. After comparison of the MCNP6, PDT, and experimental results in regards to the graphite experiments in became evident there was still a difference that could not be accounted for. The AmBe source was producing many neutrons that were being released isotopically in the experimental space. The large amount of polyethylene

in the cylinder was causing multiple neutron interactions. When comparing the MCNP6 geometry with that of the experimental setup there was a distinct characteristic missing. The missing feature was the exterior walls of the laboratory space. The MCNP6 and thus resulting PDT geometry did not contain any of the walls, floor, or celling of the experimental room. After investigation it was concluded given available information these exterior features where composed of concrete.

The neutrons interaction with concrete could cause scattered neutrons that have left the experiment to reenter the experimental setup. These neutrons scattered from the concrete would not be modeled in either MCNP6 or PDT and this could account for the difference in results between simulations and experiments. These scattered neutrons were not being taken into account during the simulation due to the use of vacuum boundary conditions. In the MCNP6 full geometry once a neutron leaves the experimental setup and travels through the air reaching the problem boundary it will exit the simulation. In PDT the same was true for the one quarter geometry of the IM1 setup. The exterior features of the laboratory space could have been added to the MCNP6 geometry. However, by adding the amount of concrete required the computational time needed to complete the simulation would increase exponentially. The same effect would have occurred during the PDT run sets and therefore it was concluded adding concrete was not the best course of action. In order to decrease computational time and still account for the neutrons scattered off the concrete walls it was determined to enclose the experimental setup in a borated polyethylene box.

The new experimental setup is displayed in Figure 3.16 below. The polyethylene box in Figure 3.17 was constructed by utilizing two sections of polyethylene on each side. The interior layer facing the experimental setup consisted of borated polyethylene. Represented by the yellow rectangles in Figure 3.17. The higher energy neutrons from the

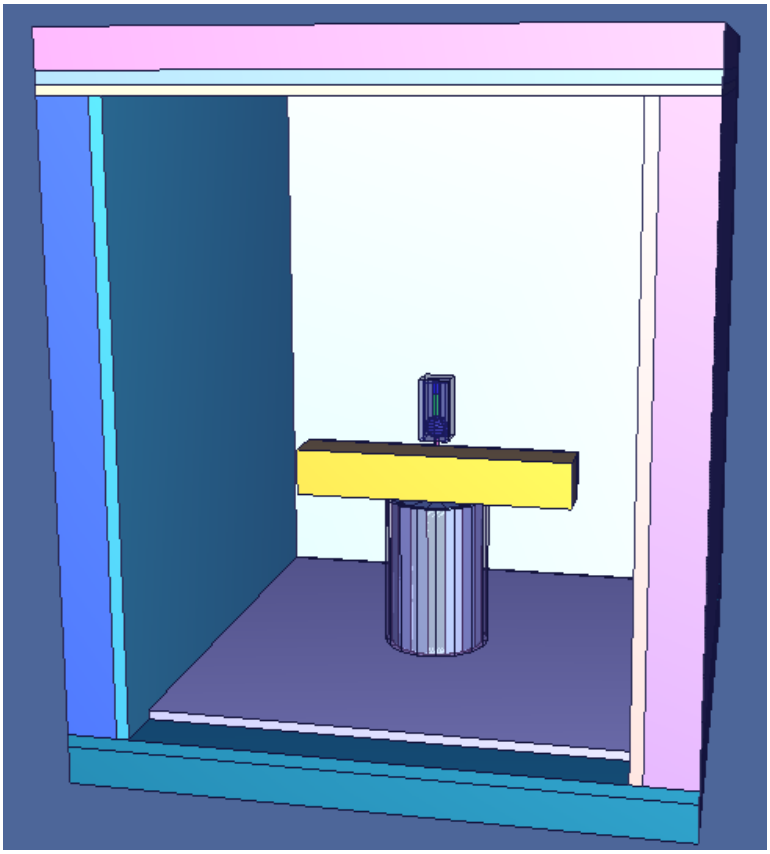

Figure 3.16: IM1 experiment with graphite bar enclosed in borated polyethylene box.

experimental setup would stream through this first layer with very little difficulty. Once the neutrons escaped the borated polyethylene they would encounter a second layer of pure polyethylene. This layer is represented by the dark blue rectangles in Figure 3.17. The layer of pure polyethylene served as a means to thermalize their energies resulting in them slowing down. In the experimental setup these neutrons would then have to scatter

off of the air in the room or the concrete exterior walls and travel back towards the polyethylene enclosure. If this was to happen the neutrons would again face thermalization in now the first layer of pure polyethylene, slowing them down further. When they reached the high absorption cross section present in the final layer of borated polyethylene these neutrons would most likely be absorbed and not permitted to reenter the experimental configuration. The addition of this experimental change would allow both MCNP6 and PDT simulations to complete with very little impact in computational time. This would largely remove the possibility of neutrons having scattered off the exterior concrete walls from reentering the experimental setup.

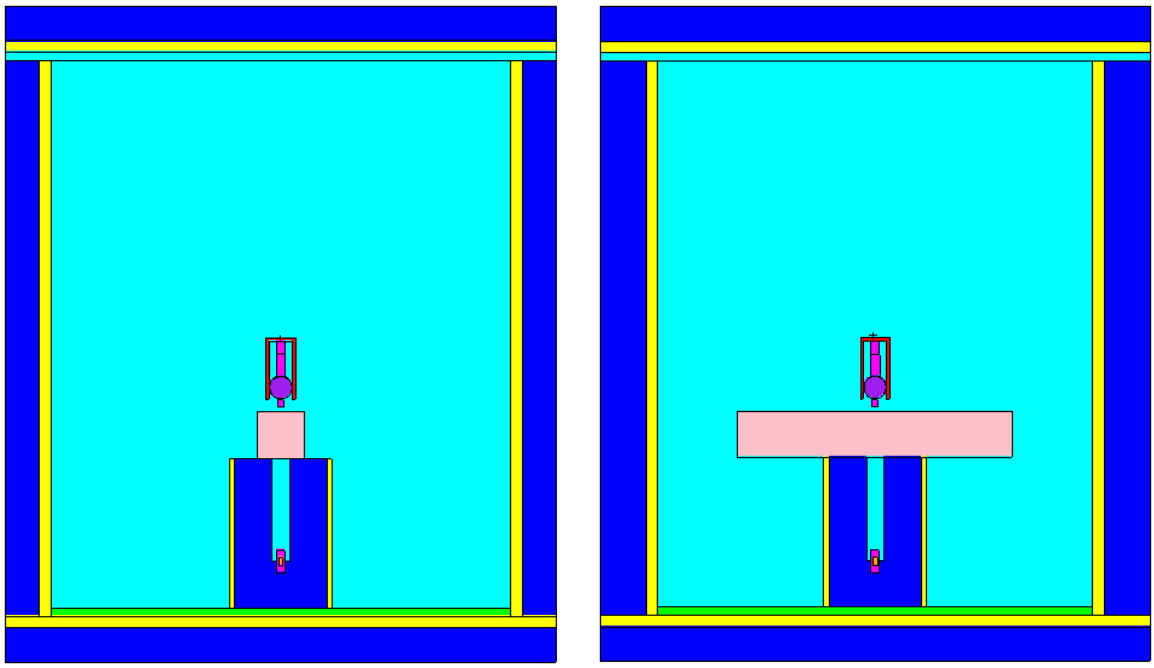

(a) (b)

Figure 3.17: Cross sections of the simulated polyethylene box enclosure of the IM1 graphite experimental geometry. The figures included are of (a) the XZ cross section of the geometry and (b) the YZ cross section of the geometry.

The inner layer of borated polyethylene was 2.5 cm in height at the top and bottom faces of the enclosure. The inner layer of borated polyethylene was 121.9 cm wide at the top and bottom faces. The inner layer of borated polyethylene was 2.5 cm wide and 122.7 cm in height for the two side faces of the enclosure. The outer pure polyethylene was 7.6

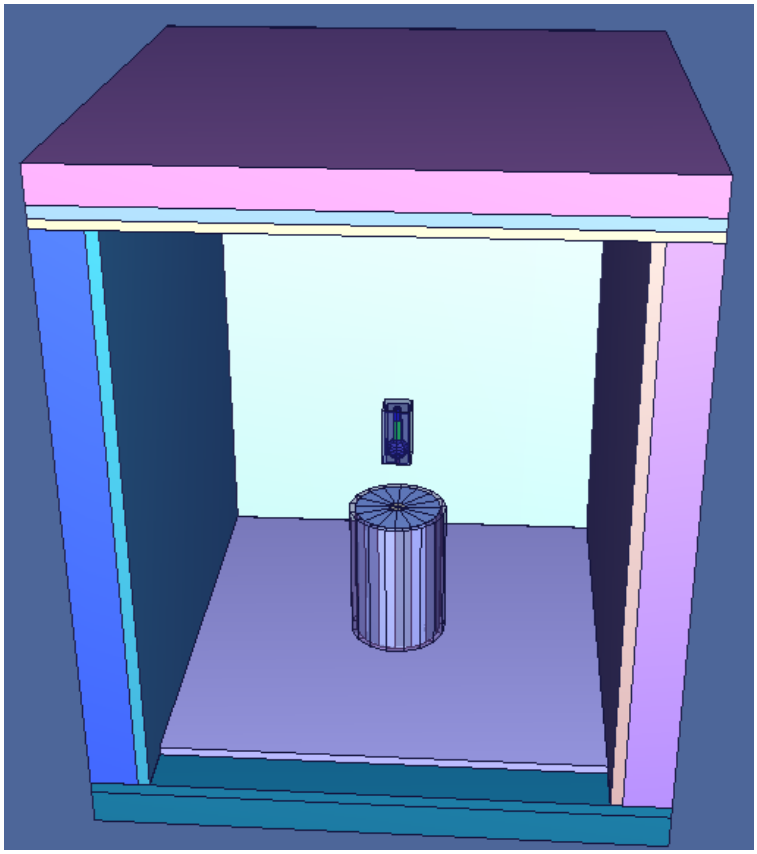

Figure 3.18: Air scenario of the IM1 experiment enclosed in borated polyethylene box.

cm in height and 121.9 cm wide at the top and bottom faces of the enclosure. The outer pure polyethylene was 122.7 cm in height and 7.6 cm wide for the two side faces of the enclosure. The measurements of the graphite block used inside the enclosure were recorded. The graphite bar used was 61 cm in length, 10.3 cm in height and 10.3 cm in

width. The same simulation was completed with the removal of the graphite bar seen in Figure 3.18 above, thus allowing only air to occupy the region.

The graphite simulation estimated 15.7 absorptions per second with 0.0025 as the relative standard error. The air simulation estimated 71.5 absorptions per second with 0.0011 as the relative standard error. Resulting in 0.219 as the graphite to air ratio for these two simulations. These geometries were made available for future use as needed. The addition of the polyethylene enclosure was an experimental change that allowed for the reduction in an unknown experimental variable. This addition allowed for the simulations using PDT and MCNP6 to be completed without the addition of concrete walls, thus preserving a large amount of computational time.

3.2 Year 5 Experiment

3.2.1 Preliminary Year 5 Experiment

The goal of this work was to refine the year 5 experiment in MCNP6 in order to visualize the effect of different neutron streaming paths. The preliminary year 5 experiment modeled a simple stacked air duct in a graphite stack. An AmBe neutron source was located in the graphite connected to the main air passageway. In order to visualize the intensity of the neutrons as they traveled throughout the preliminary geometry the FMESH card was utilized in MCNP6. This card allowed for a user defined mesh tally to be superimposed over the problem geometry. The mesh tally calculates the track length estimate of the particle flux average over a mesh cell. By utilizing the FMESH card the end results is an idea of how MCNP6 simulates neutrons streaming through different air gaps.

The preliminary year 5 geometry seen in Figure 3.19 displays the three air neutrons streaming paths represented by the three rectangles. These air ducts are located inside a stack of graphite. In Figure 3.19 on the far left face of the bottom air duct the cylindrical AmBe neutron source is simulated. During this simulation the AmBe source was

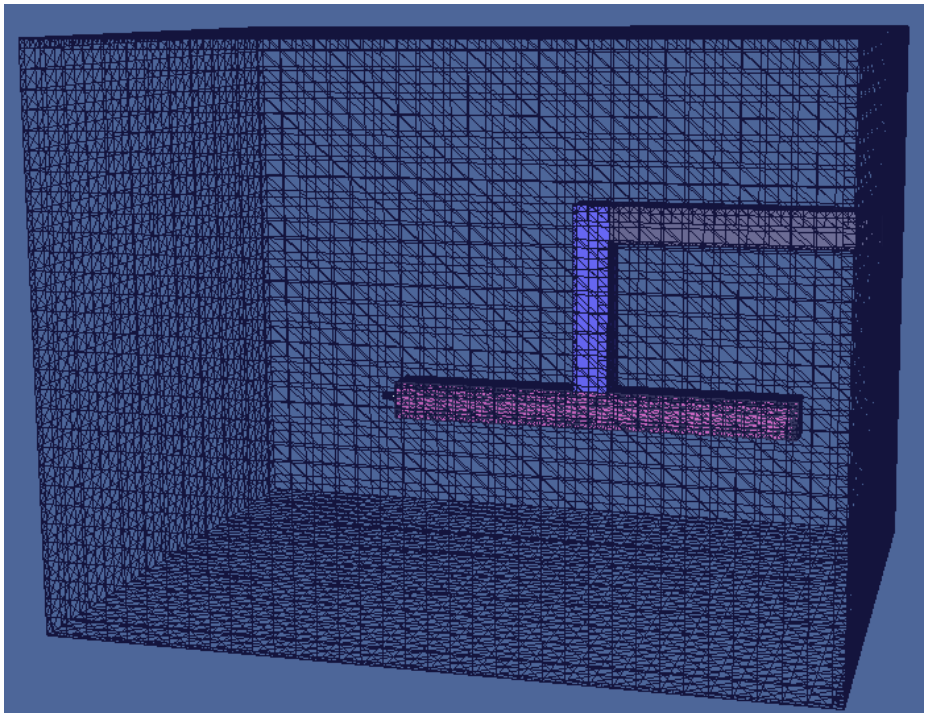

Figure 3.19: Preliminary year 5 experiment with three neutron streaming paths and a cylindrical AmBe source.

distributed isotopically. In Figure 3.20 the cross section of the full preliminary year 5 experiment is displayed. The bottom horizontal air duct was 110 cm long, 10 cm in height and 10 cm in depth. The vertical air duct was 50 cm in height, 10 cm in width, and 10 cm in depth. The top horizontal air duct was 70 cm long, 10 cm in height, 10 and cm in depth. The graphite stack represented by the green rectangle in Figure 3.20 and by the wireframe

rectangle in Figure 3.19 encompassed the air ducts and the AmBe source. The graphite stack was 150 cm in height, 200 cm long, and 150 cm in depth.

A 75 by 75 mesh was selected to be superimposed over the geometry. These 5,625 regions where equally spaced in the XY plane. For the purpose of this preliminary research the Z plane was treated as one region. This in effect utilized the FMESH card as a two dimensional representation of the geometry. The particle flux averaged over a mesh cell was recorded for each XY region and then the average overall Z directions was also recorded. This assumption was made in order to decrease the amount of computational time was needed for the simulation to complete. In Figure 3.20 the Cartesian mesh is shown superimposed over the XY cross section.

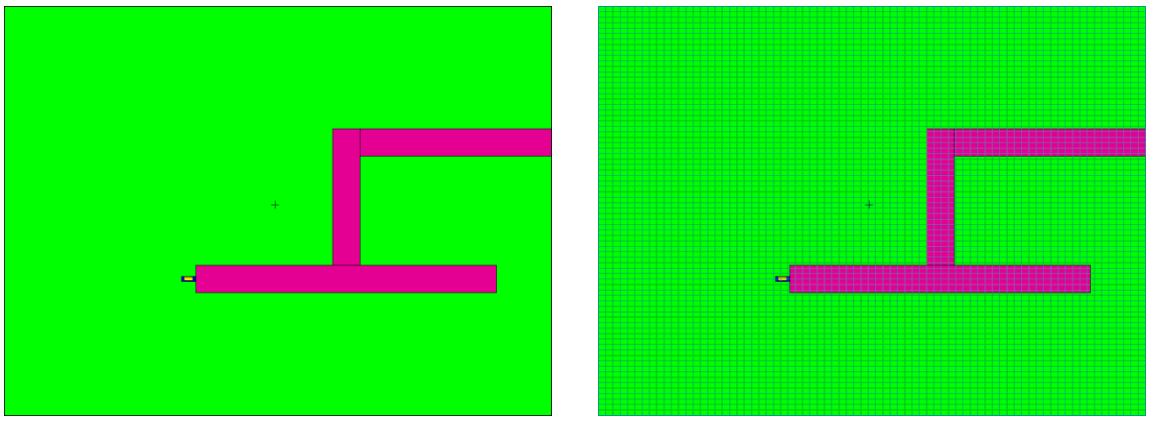

(a) (b)

Figure 3.20: Cross sections of the simulated preliminary year 5 experiment. The figures included are of (a) the XY cross section of the geometry and (b) the XY cross section of the geometry with a 75 by 75 rectangular grid overlay.

The first simulation of the preliminary year 5 geometry was completed using one billion particle histories. The result of this simulations is seen in Figure 3.21 below. Figure 3.21 displays the track length estimate of the neutron flux averaged over a mesh cell in

units of neutrons per cm^2 per source neutron. The mesh overlay in Figure 3.21 consists of the Cartesian mesh as described in Figure 3.20 above. The largest value of neutron flux averaged over a mesh cell is located at the center of the AmBe source as expected. This is represented by the small magenta circle in Figure 3.21 below. From Figure 3.21 it is apparent that the majority of neutrons traveled down the bottom horizontal air duct towards the vertical air duct. When the neutrons reached the vertical air duct a slight increase in intensity is noted by a vertical rise in the pink and purple colors towards the top horizontal air duct. At the top horizontal air duct some neutrons began to travel down the duct towards the exit of the graphite stack. From this simulation it can be concluded that the majority of neutrons will stream down the first air duct given they are born very close to it. The visualization of grey lines towards the exterior of the simulation implies

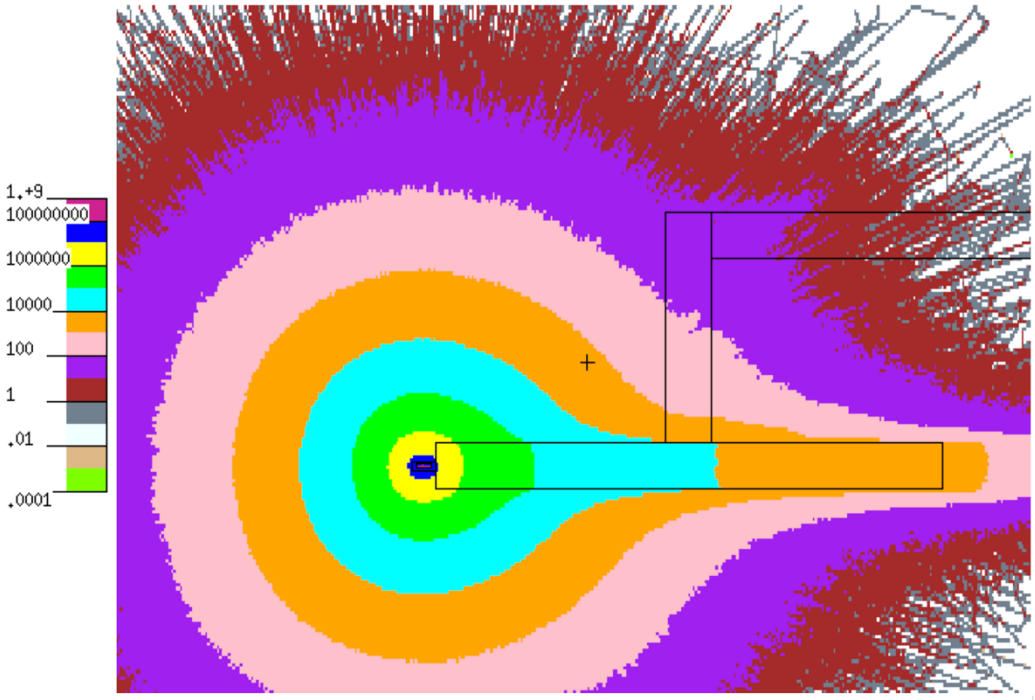

Figure 3.21: Fine Cartesian mesh neutron flux average of preliminary year 5 geometry.

the grid chosen was to fine for those regions. The simulation in Figure 3.21 was completed in 1357.64 cpu minutes. The relative standard error for this simulation is shown in Figure 3.22 below. From Figure 3.22 it is readily seen the neutron flux averaged over the mesh cells traveling down the bottom horizontal air duct has a 5% maximum relative standard error. However, as the neutrons travel up the vertical air duct the relative standard error in the track length estimate of the neutron flux averaged over a mesh cell increases drastically. By the time the neutrons have reached the top horizontal air duct the relative standard error could be up to 25% of the true value. The neutron streaming paths in the top horizontal air duct are the most unreliable. The relative standard error in this channel could be up to 100%, implying the value recorded could be incorrect. White space in

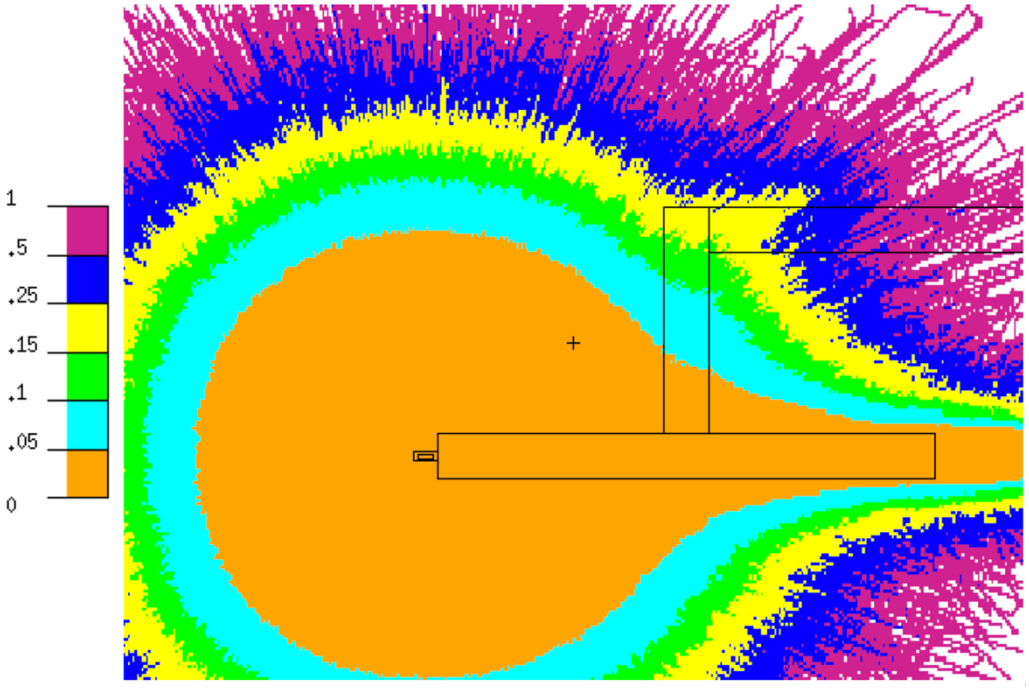

Figure 3.22: Fine Cartesian mesh relative standard error of preliminary year 5 geometry.

Figure 3.21 and Figure 3.22 is defined as having had no neutrons traveled to those mesh regions, therefore no calculation could be made. In order to decrease the relative standard error in Figure 3.21 many more neutron histories would be needed given the fine mesh grid being used. This would exponentially increase computational time and was not needed for the preliminary investigation.

An alternative to utilizing more neutron histories was modifying the mesh grid. A coarse grid of 30 by 30 regions was used in order to decrease the relative standard error and provide an additional insight on the neutron streaming paths throughout the three air

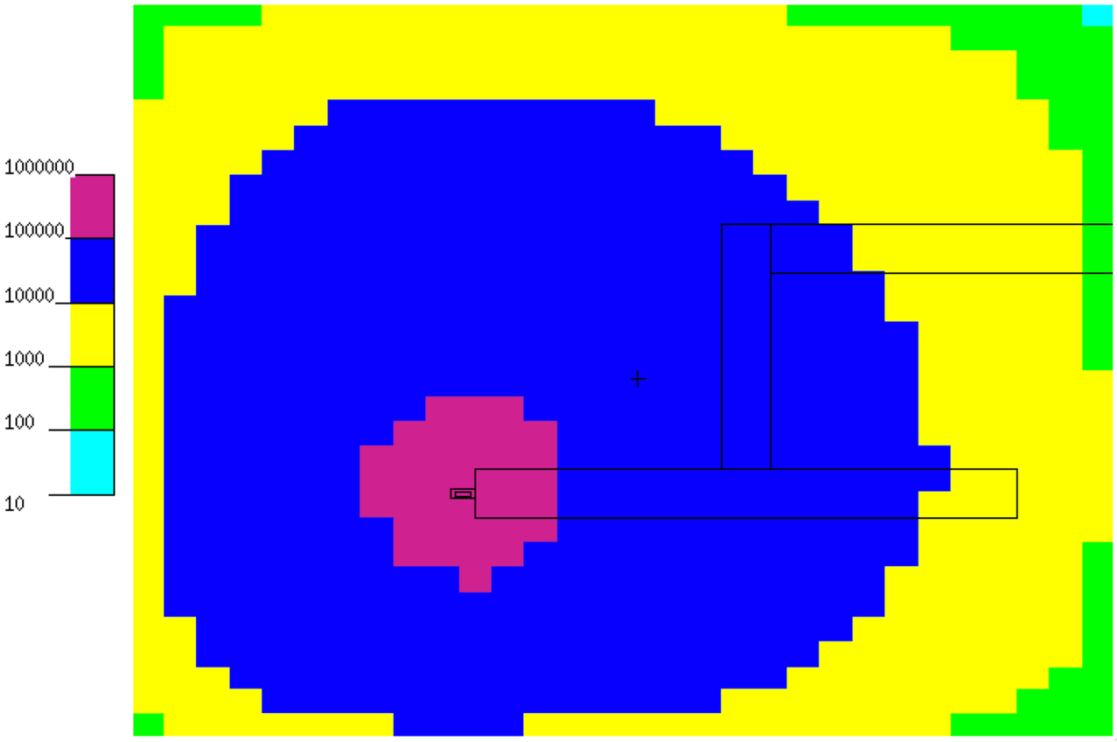

Figure 3.23: Coarse Cartesian mesh neutron flux average of preliminary year 5 geometry.

ducts. Figure 3.23 displays a coarse Cartesian mesh neutron flux average of the preliminary year 5 geometry. The coarse grid provides far less confidence that the neutrons

are being effected by the air ducts. In Figure 3.23 it is apparent that the neutron source was emitted isotopically and as distance was increased from the source the neutron flux average decreased. There is a slight deformity to the blue and yellow circles in Figure 3.23. It appears the neutron flux was larger towards the right side of the problem geometry. It could be concluded that some neutron streaming paths are being displayed and the neutrons are traveling through the air ducts. However, with very little deformity in the neutron flux average in the air ducts it is no possible to conclude neutron streaming paths were present in this coarse geometry. By reducing the number of mesh regions from 5,625 to 900 regions the relative standard error reduced to a range of 0% to 5% throughout the whole geometry. The coarse Cartesian mesh simulation was completed in 17544.12 cpu minutes.

The AmBe neutron source is emitted as a cylindrical distribution. As an additional means of visualizing the neutron streaming paths a cylindrical mesh was utilized as opposed to a Cartesian mesh. In Figure 3.24 the cylindrical mesh for the preliminary year 5 geometry is displayed. There were twenty evenly spaced circles split into 20 evenly spaced angles. This coarse cylindrical mesh results displayed in Figure 3.25 provided similar results to the coarse Cartesian mesh. The neutron flux average stayed slightly larger as the neutron streamed down the first horizontal air duct. However, when comparing these results to the expected circular distribution from an isotropic source it cannot be concluded the air ducts played a larger role. The magenta regions in Figure 3.25 are the areas where the largest neutron flux is estimated. As expected these regions surround the AmBe source. As the neutrons scatter the cylindrical mesh displays a higher

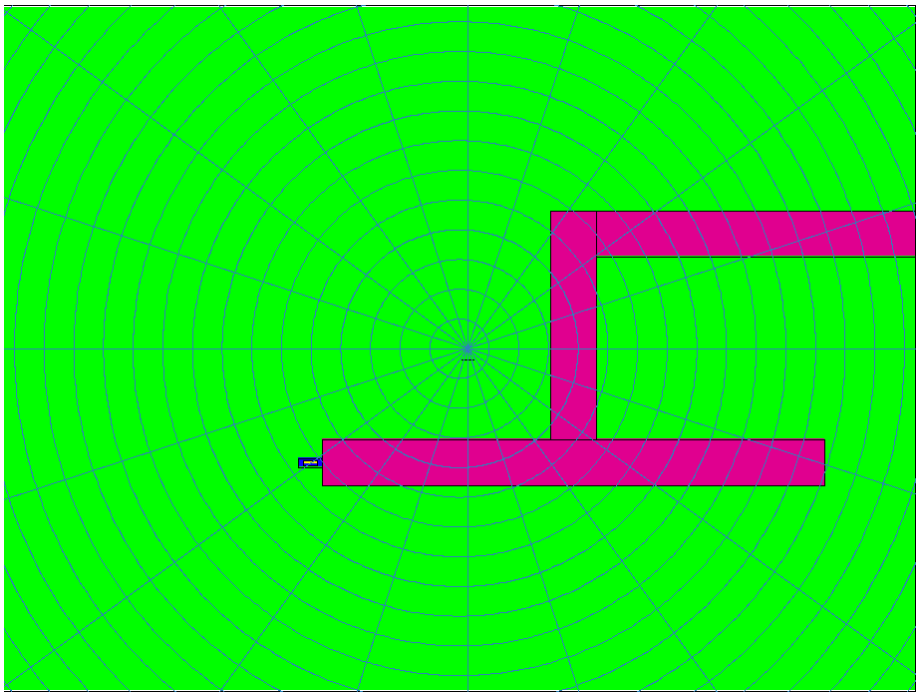

Figure 3.24: XY cross section of the simulated preliminary year 5 experiment with a cylindrical grid overlay.

neutron flux average in the air ducts then the surrounding graphite as expected. The results do not display conclusively that neutron streaming effects were present in this geometry utilizing the coarse cylindrical mesh grid. This simulation was finished in 21348.19 cpu minutes. The large computational time can be attributed to the large amount of neutrons scattering due to graphite and the need to track each neutron every step of the way. Due to the large amount of computational time already required more particle histories were not used and a finer grid was not executed. The relative standard error for the results in Figure 3.25 was 0% to 5% throughout the entire year 5 preliminary geometry. It was determined for future simulations the Cartesian mesh was the most optimal option.

The coarse mesh results from the preliminary year 5 experiment provide little confidence that MCNP6 was able to model the neutron streaming paths through the air ducts. Through monte carol techniques modeling neutron streaming paths through air ducts are extremely computationally expensive. This work completed a first pass at the future approach of how MCNP6 would be used in order to validate the streaming path predictions present in PDT.

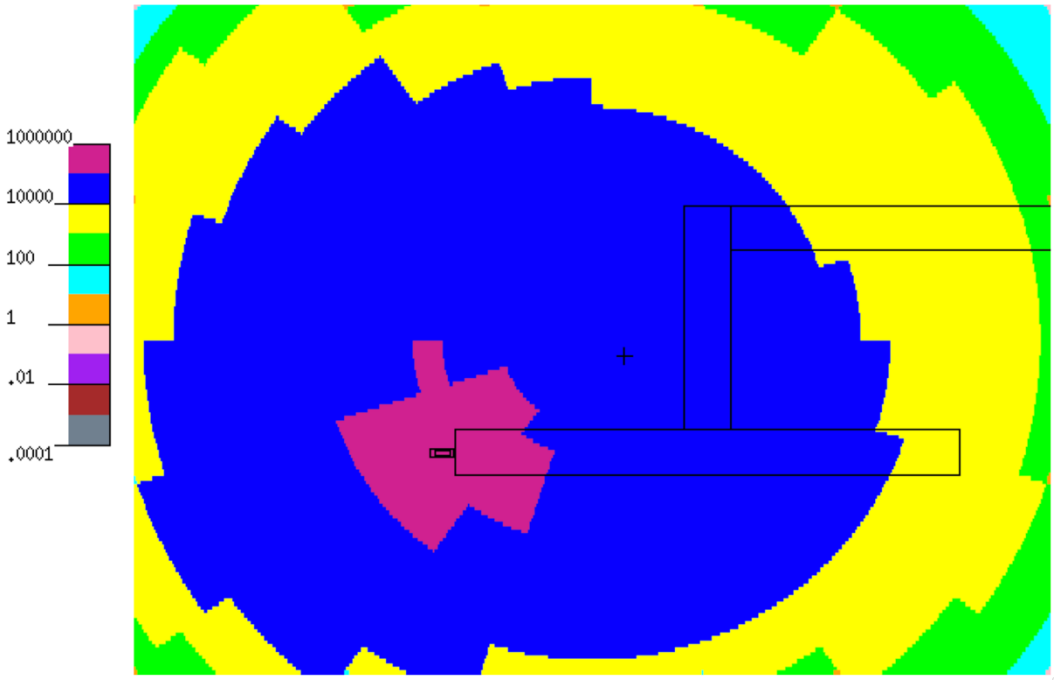

Figure 3.25: Coarse cylindrical mesh neutron flux average of preliminary year 5 geometry.

3.2.2 Year 5 Experiment with Sixty Detectors

The goal of this work was to further refine the year 5 geometries, in doing so the geometry would become asymmetric thus making the simulation more difficult to solve. Results from the preliminary year 5 experiment displayed that it was very difficult for

MCNP6 to visualize the neutron streaming paths. A more complex geometry will make these streaming paths far more difficult to visualize and therefore another approach was taken to solve this challenge. The same stacked air duct that was used in the preliminary geometry was also used in this more complex geometry with minor modifications. Three thin slits where interested into the graphite stack that aligned with the air ducts introducing another unknown to the simulation. For this simulation the same AmBe source was utilized as it was the only neutron source available at the time. This geometry was produced in order to challenge both the MCNP6 code as well as the PDT code.

In Figure 3.26 and Figure 3.27 the year 5 experiment with sixty detectors is fully represented. The three air ducts are located inside the graphite stack. The graphite stack is

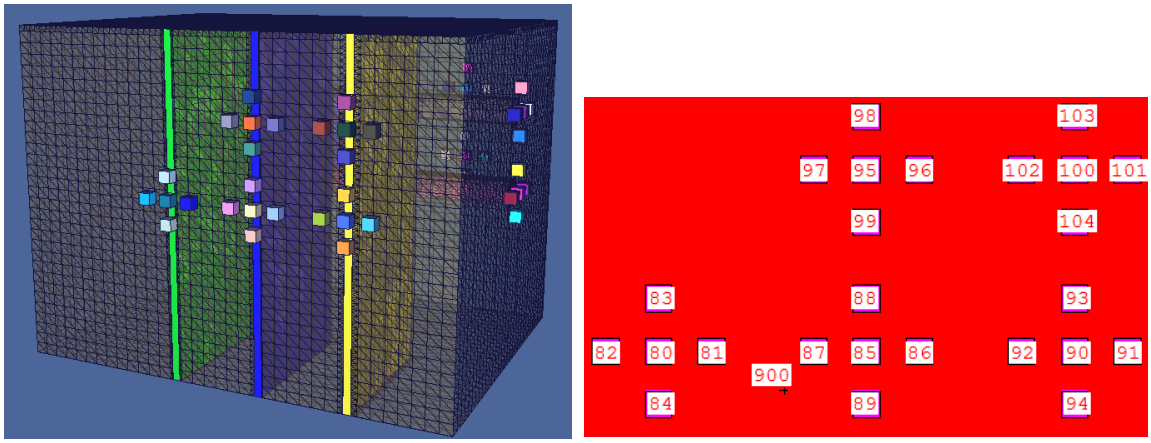

(a) (b)

Figure 3.26: Simulated geometry of year 5 experiment with sixty detectors. The figures included are of (a) the face of the geometry with air slits extruding from the graphite stack and (b) the corresponding detector number.

represented in Figure 3.26 by the wire frame box. On the outside of the graphite stack is twelve groups of five detectors in a cross formation. These individual detectors make up

the sixty detectors that surrounded the experiment. There is a layer of air that is simulated outside the graphite stack all around the experiment including the sixty detectors. This geometry was used to predict where the most neutron absorptions would be present in order to place the detectors during the experimental setup. The bottom horizontal air duct

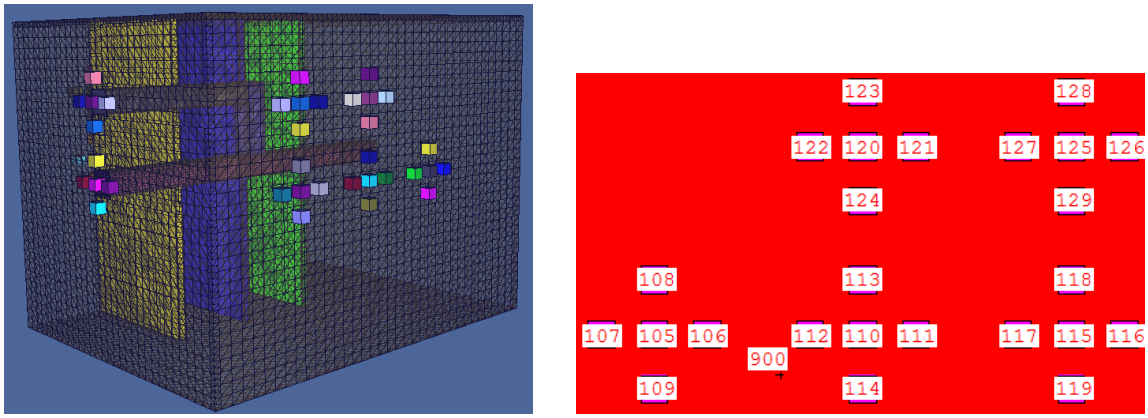

(a) (b)

Figure 3.27: Simulated geometry of year 5 experiment with sixty detectors. The figures included are of (a) the face of the geometry where detectors are on the graphite stack with no air slits and (b) the corresponding detector number.

is 168 cm long, 10.1 cm in height, and 10.1 cm in depth. The vertical air duct is 34.9 cm in height, 10.1 cm in width, and 10.1 cm in depth. The center of the vertical air duct is located 85.1 cm from the closest end of the AmBe source. The top horizontal air duct is 78.8 cm long, 10.1 cm in height, and 10.1 cm in depth. These three air ducts were modified from the preliminary geometry due to experimental change and the results from the first geometry. The graphite stack represented by the wire frame in Figure 3.26 was 200 cm in length, 150 cm in height, and 150 cm in depth. Inside the graphite stack was three air slits that spanned the length of the air ducts to the exterior of the graphite stack. These air slits

are represented in Figure 3.26 and Figure 3.28 by the thin green, blue, and yellow rectangles. Each rectangle is 150 cm in height, 3.4 cm in width, and 69.9 cm in depth.

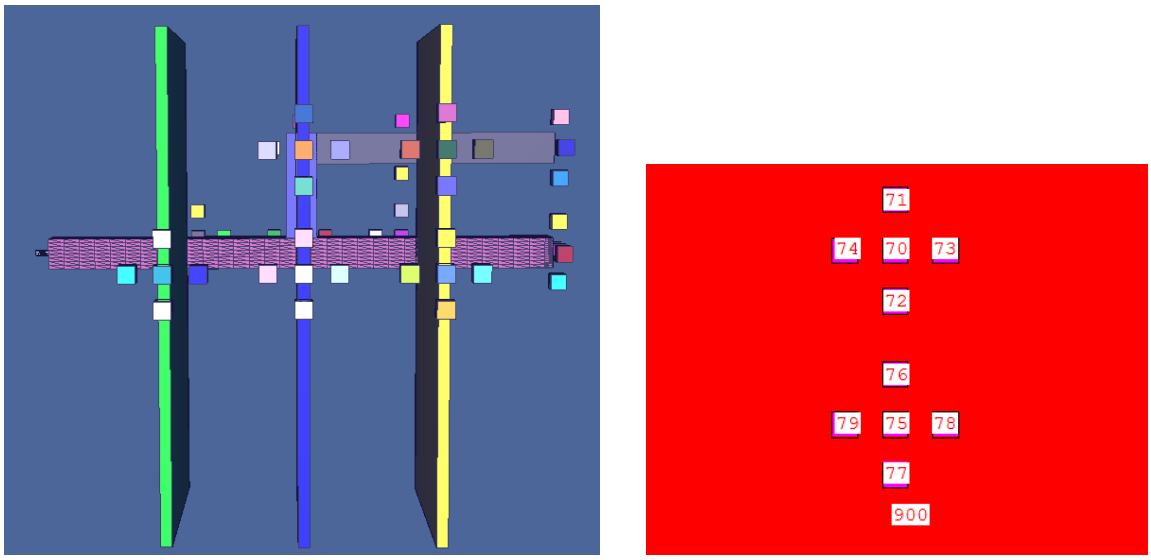

(a) (b)

Figure 3.28: The figures included are of (a) View of air channels for the year 5 geometry with sixty detectors and (b) head on view with corresponding detector numbers.

The center of the green air slit is located 45.1 cm away from the near end of the AmBe source. The center of the blue air slit is in line with the vertical air duct and is 85.1 cm away from the near end of the AmBe source. The yellow air slit is located 125.1 cm away from the near end of the AmBe source. The sixty detectors are each identically represented throughout this geometry. The detectors are cubes where each side is 5.1 cm in length. These detectors were modeled as simplified BF_3 detectors.

The simulation was completed with ten billion particle histories using 656 processors on CAB at LLNL. This simulation was completed in 259.2 cpu days. The simulation results for each detector is displayed in Figure 3.29 where the intensity of color

corresponds to the amount of absorptions per second recorded in the detector volumes. Table 3.3 also displays the results of the 60 detectors in a numerical form. From Table 3.3 it is concluded detector 80 had the largest simulated absorptions per second of 384.4 with a relative standard error of 0.0004 for the simulation. This detector was located in tally volume 80 as seen in Figure 3.26. This detector is represented in Figure 3.28 as a teal cube in the center of the group of five detectors located in line with the green air slit. This detector is also in line with center of the bottom horizontal air duct. These results align with the expected outcome. The neutrons from the AmBe source will scatter through the graphite as well as travel up the nearest air slit causing the most simulated absorptions per second. The two next largest absorptions per second value of 378.4 and 372.6 are located below and above the center detector on the green air slit respectively. The relative standard error was 0.0004 for each of these two detectors. These detectors are located in tally region 84 and 83 found in Figure 3.26. As you move towards the edge of the graphite away from the AmBe source the absorption per second values decrease rapidly. The detector centered on the bottom horizontal air duct in line with AmBe source simulated 71.8 absorptions per second with 0.009 as the relative standard error. This was expected as the neutrons had a long distance to travel through the air duct or graphite and from the preliminary year 5 results. The detectors along the air slits simulated decreasing absorptions per second as they were located farther away from the source. The detector centered on the top horizontal air duct simulated 45.3 absorptions per second with 0.0011 as the relative standard error.

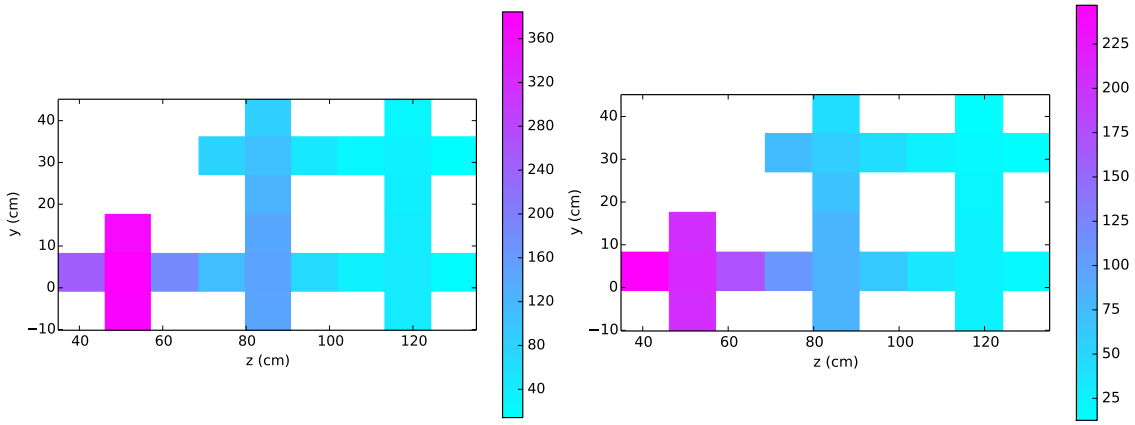

(a) (b)

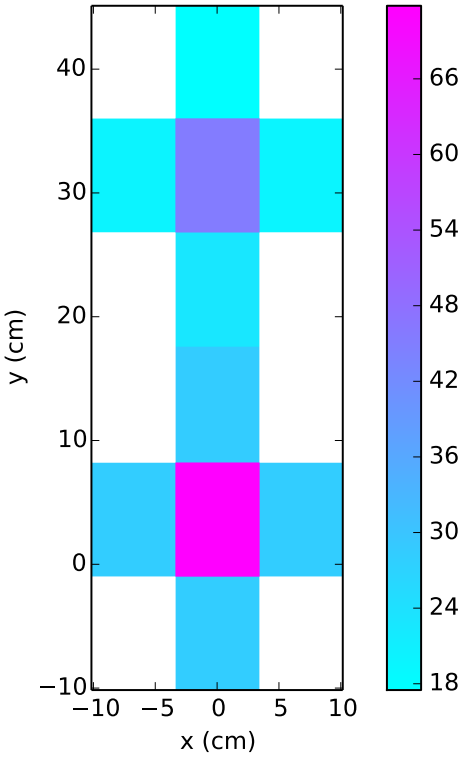

(c)

Figure 3.29: The absorptions per second for each of the sixty detector locations. The figures included are of (a) the 25 detectors located on the air slits, (b) the 25 detectors located opposite of the air slits on the graphite block, and (c) the ten detectors located on the end of the air ducts.

Table 3.3: Year 5 geometry with 60 detectors simulated absorptions per second values.

Detector Tally Region	Absorptions/Second	RSE	Error
70	45.3	0.0011	0.050
71	17.5	0.0018	0.032
72	22.8	0.0016	0.036
73	19.8	0.0017	0.034
74	19.9	0.0017	0.034
75	71.8	0.0009	0.065
76	28.5	0.0014	0.040
77	28.3	0.0014	0.040
78	28.3	0.0014	0.040
79	28.2	0.0014	0.040
80	384.4	0.0004	0.154
81	184.4	0.0006	0.111
82	249.1	0.0005	0.125
83	372.6	0.0004	0.149
84	378.4	0.0004	0.151
85	146.3	0.0006	0.088
86	67.6	0.0009	0.061
87	109.1	0.0008	0.087
88	141.8	0.0006	0.085
89	144.5	0.0006	0.087
90	44.1	0.0011	0.049
91	19.7	0.0017	0.034
92	35.5	0.0013	0.046
93	42.9	0.0011	0.047
94	43.7	0.0011	0.048
95	105.4	0.0007	0.074
96	47.9	0.0011	0.053
97	76.6	0.0009	0.069
98	83.4	0.0008	0.067
99	124.1	0.0007	0.087
100	32.3	0.0013	0.042
101	14.2	0.0021	0.030
102	25.3	0.0016	0.040
103	25.8	0.0015	0.039
104	37.9	0.0012	0.045
105	210.0	0.0005	0.105
106	172.3	0.0006	0.103
107	246.9	0.0005	0.123
108	203.0	0.0006	0.122
109	205.8	0.0006	0.123
110	82.4	0.0009	0.074
111	62.0	0.0010	0.062
112	108.3	0.0008	0.087
113	79.7	0.0009	0.072
114	81.3	0.0009	0.073
115	24.9	0.0015	0.037
116	17.6	0.0018	0.032
117	34.7	0.0013	0.045
118	24.2	0.0016	0.039
119	24.8	0.0015	0.037
120	57.2	0.0010	0.057
121	43.3	0.0012	0.052
122	74.7	0.0009	0.067
123	43.6	0.0012	0.052
124	69.0	0.0009	0.062
125	17.7	0.0018	0.032
126	12.6	0.0022	0.028
127	24.5	0.0016	0.039
128	13.7	0.0021	0.029
129	21.2	0.0017	0.036

These results were completed without any experimental data to compare them against. This geometry was made available to PDT in order for the same problem to be simulated and the results compared in the future. The results also showed the neutrons streaming paths may be predicted, however this high fidelity of results is extremely computationally expensive. Even though the simulation is computationally expensive there is relative standard error present for each detector volume. These results suggest the most efficient placement of BF_3 detectors for future experimental trials would be centered on the air slits as well as centered on the exit of both the top and bottom horizontal air duct.

3.3 Neutron Generator Safety Calculations

The goal of this work was to simulate the amount of dose that would be expected to operating and witnessing personnel given the neutron generator was placed in the existing laboratory space. The neutron generator simulated is described as producing a pulse of 14.1 MeV neutrons 98% of the time and 2.5 MeV neutrons the remaining 2% of the time. The neutron generator was still being delivered during these simulations therefore the source definition was defined given the available information. The neutron generator as defined in the purchase order will produce 3×10^9 neutrons per second, minimum at maximum pulse rate. Therefore this was the source strength used in the simulation as the neutron generator is cable of sustaining 3×10^9 neutrons per second when operating at maximum pulse rate.

The laboratory room is defined thoroughly in Section 2.3 above. The simulated geometry is displayed in Figure 3.30 below. In order to simulate the dose a person would

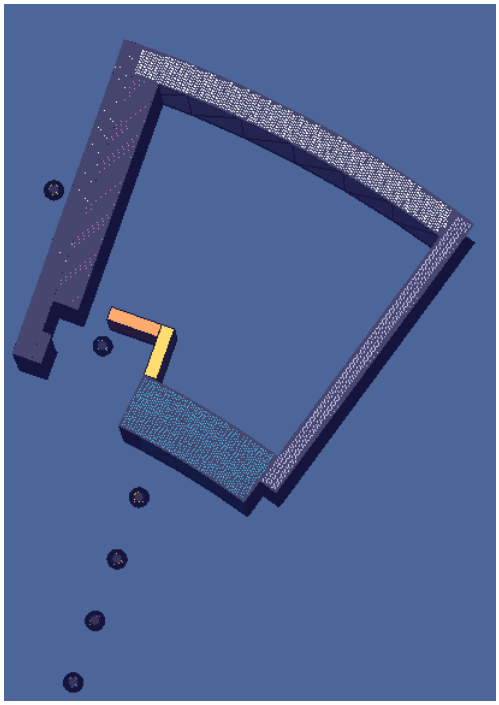

Figure 3.30: Simulated geometry of laboratory room utilized for the neutron generator.

receive four phantom sphere were located in the main concourse leading to the laboratory room. One phantom sphere was located in the center of the adjoining room near the concrete separating wall. One phantom sphere was located inside the door leading to the laboratory room. These phantom spheres are represented in Figure 3.30 by the six spheres. Every supporting structure in Figure 3.30 is made of concrete. The floor and ceiling is modeled as concrete; they are not represented in Figure 3.30 in order to increase detail on the salient features.

A cross section representation of the geometry is displayed in Figure 3.31 below. In order to decrease the amount of dose being simulated shielding was added inside and outside the laboratory space. This concrete shielding in Figure 3.31 is labeled as structures

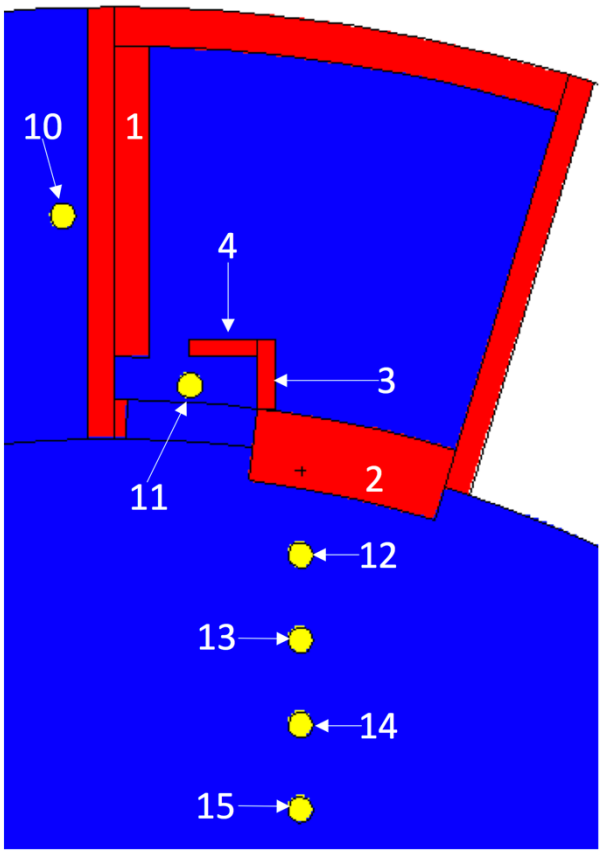

Figure 3.31: Cross section of simulated geometry of laboratory room being utilized for experiments.

one through four. The concrete shielding denoted as structure one is stacked inside the laboratory space against the wall that is separating the adjoining room. This concrete is 40.6 cm thick along the wall. There is no concrete shielding on the opposite wall as this leads to soil and will not be accessible to any person. The concrete shielding represented as structure two is located outside of the laboratory space against the hallway to the right of the exterior door. This concrete shielding is also 40.6 cm thick. The shielding was chosen to be 40.6 cm thick due to the availability of concrete blocks that fit this specification on hand. The concrete shielding denoted as structure three is the vertical

section of the ‘L’ shaped shielding located inside the room. This structure is 20.3 cm thick, 198.1 cm in height, and 81.3 cm long spanning towards the center of the room. The fourth structure as represented in Figure 3.31 is the horizontal section of the ‘L’ shaped shielding located inside the room. This section of shielding is 20.3 cm thick, 198.1 cm in height, and 81.3 cm long spanning towards the wall that leads to the adjoining room. There is a 47.0 cm gap between structure one and structure four to allow personnel to enter or exit the laboratory room when the experiment is not operating. The phantom spheres are structures numbered 10 through 15 in Figure 3.31 above. Sphere 10 is located 367 cm away from the neutron generator source. Sphere 11 located inside the door is 270 cm away from the neutron generator source. Sphere 12 is located 360 cm away from the neutron generator source. Sphere 13, 14, and 15 are each 460 cm, 560 cm, and 660 cm away from the neutron generator source respectively. These phantom spheres are standardized with a 15 cm radius consisting of normal water.

The neutron generator source is approximated as an isotropic source with two discrete energies. From available documentation a 2.5 MeV neutron history was to be born 2% of the time and a 14.1 MeV neutron history was to be born 98% of the time. There were 500 million neutron histories generated in order to decrease relative standard error while not utilizing excessive computational time. A dose function card was used to authorize MCNP6 to utilize a standard flux-to-dose conversion factor as a function of energy to modify a regular tally. These factors where performed on the flux computed in each of the six phantom spheres. The dose function input card for MCNP6 allowed for the dose to be estimated in each phantom sphere in units of mrem per hour. Based on expert

opinions and current research the dose function for neutrons was chosen. These simulations utilized the NCRP-38 1971, ANSI/ANS-6.1.1-1977 neutron dose function values found in Table A1 in Appendix A.

The simulated dose rate for each sphere is displayed in Table 3.4 below. As expected sphere 11 referenced in Figure 3.31 had the largest simulated dose rate. This phantom sphere is located inside the laboratory room while the neutron generator is

Table 3.4: Simulated dose results for neutron generator safety calculations.

Phantom Sphere	mrem/hr	Absolute Error
10	1.06	0.027
11	107.04	0.300
12	4.24	0.050
13	4.72	0.054
14	3.79	0.049
15	2.90	0.044

operating with very little shielding present. The other five sphere locations all simulated dose rates of less than five mrem per hour. This low dose rate concludes the simulated shielding is sufficient for primary experimental trials to begin. The MCNP6 simulation will need to be modified once the neutron generator has arrived on site and the neutron pulse specifications are clarified. These simulations were meant to provide operating and witnessing personnel an estimation of the amount of dose they would be receiving. These simulations should be confirmed by the area safety officer and additional dose measurements should be taken to validate the MCNP6 results.

4. CONCLUSIONS AND FUTURE WORK

4.1 Conclusions

In conclusion, multiple MCNP6 simulations were completed to support the validation of PDT development. The simulated results were presented in Section 3 above. After analysis it was determined the 115 group SOURCES 4A AmBe neutron source definition was the most accurate source definition for use in MCNP6 and PDT. This source definition provided the most stability for initial results. The 115 group SOURCES 4A definition also represented the expected AmBe neutron spectrum with greater precision and had a steadfast reference which it was derived from.

Six different graphite block and BF_3 detector orientations were simulated outside of a polyethylene box. The five alternative arrangements and one standard arrangement could each provide additional insight in how MCNP6 is tracking neutrons and determine the absorptions per second in each detector volume. With the addition of multiple detectors in one geometry PDT and MCNP6 run times could be reduced drastically. These completed geometries will aid in efficiency when their results are required.

The IM1 model was simulated inside a polyethylene enclosure in order to represent the new experimental setup. Once the setup was simulated inside the enclosure the BF3 detector simulated 15.7 ± 0.039 absorptions per second when the graphite block was present. The standard IM1 configuration with no graphite block simulated 71.5 ± 0.079 absorptions per second.

Thirteen distinct boric acid concentrations were completed during the simulation. Each boric acid concentration required its own specific MCNP6 input deck. As the

concentration of boric acid was increased in the beaker a decreasing exponential trend in the absorptions per second the BF_3 detector recorded was visualized. Many neutron histories were sampled such that the relative standard error was less than one percent for each distinct concentration of boric acid. With just water present in the beaker the BF_3 detector simulated 6.288 ± 0.025 absorptions per second. With a boric acid concentration of 600 ppm the BF_3 detector simulated 4.576 ± 0.022 absorptions per second.

The preliminary year 5 experimental geometry was simulated in MCNP6. This simple geometry allowed for neutron streaming figures to be created. These figures provided little confidence that MCNP6 was able to model the effect neutron streaming paths had on the graphite stack. The more complex year 5 geometry with air slits and 60 detectors, in addition to stacked air ducts was completed. From this geometry it became apparent that the center of the first air slit and the exit of each of the two air ducts simulated the most absorptions per second in the simplified BF_3 detectors. The simulation was completed in 259.2 cpu days. These results provided insight that MCNP6 can model the addition of neutron streaming paths, however it is extremely computationally expensive.

The final simulation completed was that of the neutron generator safety calculations. During these simulations it was concluded specific concrete shielding needed to be added to the laboratory room. With the addition of the shielding the estimated dose in the entrance way to the room was 107.04 mrem per hour. There will be no employee standing in the doorway during neutron generator operation. It was also concluded that in the hallway the estimated dose was 4.72 mrem per hour during operation. The simulated results and geometry were made available.

4.2 Future Work

Future work should contain multiple MCNP6 and PDT simulations. The correct source definition concluded upon should be implemented into each graphite configuration input deck as well as any future simulations. The alternative graphite and BF_3 detector configurations should be updated to be enclosed by the polyethylene box. The boric acid experiment should be simulated inside the polyethylene box in the future. Once the neutron generator arrives on site the year 5 and safety calculations should be updated. The year 5 experiment geometries could be updated to include a more precise definition of the neutron generator. The year 5 geometry should also more accurately represent the specific experimental setup being utilized. The year 5 geometry would be modified to only include the detector locations used and more detailed BF_3 detectors would be modeled. Finally, the neutron generator safety calculations should be refined in order to account for specific neutron generator details and laboratory room setup.

REFERENCES

Los Alamos National Laboratory. *MCNP6TM USER'S MANUAL*. Los Alamos , 1 May 2013.

Technical Committee ISO/TC 85, Nuclear energy, Subcommittee SC 2, Radiation protection. *ISO 8529-2:2000 Reference neutron radiations -- Part 2: Calibration fundamentals of radiation protection devices related to the basic quantities characterizing the radiation field*. 2016.

Knoll, Glenn. *Radiation Detection and Measurement*. Fourth Edition. Hoboken: John Wiley & Sons, Inc. , 2010.

Relly, Doug, Ensslin Norbert, and Smith Norbert , Jr. *Passive Nondestructive Assay of Nuclear Materials*. Ed. Sarah Kreiner. Los Alamos: Los Alamos National Laboratory, 1991.

Turner, James E. *Atoms, Radiation, and Radiation Protection*. Third Edition. Oak Ridge: WILEY-VCH Verlag GmbH & Co. KGaA, Weinheim, 2007.

APPENDIX A

DOSE CONVERSION

This section contains the dose conversion factors utilized during the MCNP6 simulations for the safety calculations.

Table A1: Neutron Flux-to-Dose Rate Conversion Factors and Quality Factors.

	NCRP-38, ANSI/ANS-6.1.1-1977	
Energy, E (MeV)	**DF(E) (rem/hr)/(n/cm2-s)**	**Quality Factor**
2.50E-08	3.67E-06	2.0
1.00E-07	3.67E-06	2.0
1.00E-06	4.46E-06	2.0
1.00E-05	4.54E-06	2.0
1.00E-04	4.18E-06	2.0
1.00E-03	3.76E-06	2.0
1.00E-02	3.56E-06	2.5
1.00E-01	2.17E-05	7.5
5.00E-01	9.26E-05	11.0
1.0	1.32E-04	11.0
2.5	1.25E-04	9.0
5.0	1.56E-04	8.0
7.0	1.47E-04	7.0
10.0	1.47E-04	6.5
14.0	2.08E-04	7.5
20.0	2.27E-04	8.0